EFFECT OF STRAIN RATE ON STRENGTH AND DEFORMABILITY OF MAHA SARAKHAM SALT

Prapasiri Junthong

A Thesis Submitted in Partial Fulfillment of the Requirements for the

Degree of Master of Engineering in Geotechnology

Suranaree University of Technology

Academic Year 2016

ผลกระทบของอัตราความเครียดต่อกำลังและการเสียรูปของเกลือหินชุดมหาสารคาม

นางสาวประภาศิริ จั่นทอง

วิทยานิพนธ์นี้เป็นส่วนหนึ่งของการศึกษาตามหลักสูตรปริญญาวิศวกรรมศาสตรมหาบัณฑิต
สาขาวิชาเทคโนโลยีธรณี
มหาวิทยาลัยเทคโนโลยีสุรนารี
ปีการศึกษา 2559

EFFECT OF STRAIN RATE ON STRENGTH AND DEFORMABILITY OF MAHA SARAKHAM SALT

Suranaree University of Technology has approved this thesis submitted inpartial fulfillment of the requirements for a Master's Degree.

Thesis Examining Committee

_____

(Assoc. Prof. Dr. Pornkasem Jongpradist)

Chairperson

_____

(Asst. Prof. Dr. Decho Phueakphum)

Member (Thesis Advisor)

_____

(Prof. Dr. Kittitep Fuenkajorn)

Member

_____

(Prof. Dr. Sukit Limpijumnong)

Vice Rector for Academic Affairs and Innovation

_____

(Assoc. Prof. Flt. Lt. Dr. Kontorn Chamniprasart)

Dean of Institute of Engineering

ประภาศิริ จั่นทอง : ผลกระทบของอัตราความเครียดต่อกำลังและการเสียรูปของเกลือหินชุดมหาสารคาม(EFFECT OF STRAIN RATE ON STRENGTH AND DEFORMABILITY OF MAHA SARAKHAM SALT)อาจารย์ที่ปรึกษา : ผู้ช่วยศาสตราจารย์ ดร.เดโชเผือกภูมิ, 65หน้า.

วัตถุประสงค์ของงานวิจัยคือเพื่อหาค่ากำลังและการเสียรูปของเสาค้ำยันในเหมือง เกลือในระยะยาวได้ดำเนินการทดสอบกำลังรับแรงกดในแกนเดียวและในสามแกนภายใต้การผันแปรอัตราความเครียดในแนวแกนคงที่บนตัวอย่างเกลือหินมีการผันแปรความเค้นล้อมรอบ ตั้งแต่ 0, 3, 7 และ 12 เมกะปาสคาลอัตราความเครียดในแนวแกน ผันแปรระหว่าง 10^{-7}ถึง 10^{-4}ต่อวินาทีได้ควบคุมอัตราความเครียดในแนวแกนด้วยมาตรวัดการเคลื่อนตัวและทำการบันทึกค่า กำลัง ในแนวแกนและค่าความเครียดในแนวด้านข้าง เป็นระยะเวลาถึง 21 วัน ผลการทดสอบ ระบุ ว่า ค่า กำลัง และค่าสัมประสิทธิ์ความยืดหยุ่น มีค่าเพิ่มขึ้นเมื่ออัตราความเครียดในแนวแกนเพิ่มขึ้น ได้ทำการ สอบเทียบผลการทดสอบกับสมการความคืบแบบยกกำลังเพื่อหาค่าตัวแปรเชิงคณิตศาสตร์ โดยข้อมูลดังกล่าวสามารถนำมาสร้าง กราฟความสัมพันธ์ระหว่าง ค่าความเครียดของเสาค้ำยัน เชิงเวลา ภายใต้การผันแปรความลึกของช่องเหมืองและอัตราการขุดเจาะแร่เนื่องจากการศึกษาได้พิจารณาทั้งกำลังและความเครียด ดังนั้นจึงสามารถพัฒนาเกณฑ์การแตกในรูปแบบของพลังงานความเครียดเชิงเบี่ยงเบนเพื่อใช้ในการประเมินเสถียรภาพของเสาค้ำยัน โดยผลการคำนวณระบุว่าค่าพลังงานความเครียดเชิงเบี่ยงเบนของเกลือหินในช่วงที่เริ่มมีการเปลี่ยนแปลงรูปร่างและในช่วงที่เกิดการแตกมีค่าผันแปรเชิงเส้นกับค่าความเค้นเฉลี่ย เมื่อนำข้อมูลจากราฟความสัมพันธ์ระว่างค่าความเครียดของเสาค้ำยันในเชิงเวลาภายใต้การผันแปรความเค้นต่างๆมาคำนวณค่าพลังงานความเครียดเชิงเบี่ยงเบนและนำไปเทียบกับกราฟความสัมพันธ์ของพลังงานความเครียดดังกล่าว จึงทำให้สามารถคาดคะเนระยะเวลาของเสาค้ำยันก่อนที่จะเกิดการพังได้

สาขาวิชาเทคโนโลยีธรณี ลายมือชื่อนักศึกษา _____

ปีการศึกษา2559 ลายมือชื่ออาจารย์ที่ปรึกษา_____

PRAPASIRI JUNTHONG: EFFECT OF STRAIN RATE ON STRENGTH AND DEFORMABILITY OF MAHA SARAKHAM SALT.
THESIS ADVISOR:ASST. PROF.DECHO PHUEAKPHUM, Ph.D., 65 PP

DILATION/FAILURE/ELASTIC MODULUS/STRAIN RATE/TIME-DEPENDENT

The objective of this study is to determine the long-term strengthsand deformations of pillars in salt mines in the northeast of Thailand. Strain rate-controlled uniaxial and triaxial compression tests have been performed on salt specimens.The confining pressures are maintained constant ranging from 0, 3, 7 to 12 MPa. The applied strain rates are varied from 10^{-7} to 10^{-4} s^{-1}.The axial strain rate are monitored and controlled using dial gage and the axial stresses and lateral strains are recorded through the strain-softening region for up to 21 days. The results indicate that the strengths and elastic moduli increase exponentially with the applied strain rates. The potential law parameters are calibrated with the test results, and hence allows constructing series of strain-time curves for the pillars subjected to vertical stresses under different depths and extraction ratios. To consider both stress and strain, the strain energy density principle is applied to develop strength criterion for the salt pillars. It is found that the distortional strain energy at dilation and at failure varies linearly with the mean stress (σ_m). Combining this criterion with the series of the strain-time curves the time-dependent strengths of the salt pillars can be predicted.

School of Geotechnology Student's Signature_____

AcademicYear 2016 Advisor's Signature_____

ACKNOWLEDGMENTS

I wish to acknowledge the funding supported by Suranaree University of Technology (SUT).

I would like to express my sincere thanks to Prof. Dr. KittitepFuenkajorn for his valuable guidance and efficient supervision. Iappreciate his strong support, encouragement, suggestions and comments during the research period. My heartiness thanks toAssoc. Prof. Dr. Pornkasem Jongpradist, Asst. Prof. Dr. DechoPhueakphum,and Dr. Prachya Tepnarongfor their constructive advice, valuable suggestions and comments on my reseach works as thesis committee members.Grateful thanks are given to all staffs of Geomechanics Research Unit, Institute of Engineering who supported my work.

Finally, Iwould like to thank beloved parents for their love, support and encouragement.

Prapasiri Junthong

TABLE OF CONTENTS

Page

TABLE OF CONTENTS (Continued)

Page

TABLE OF CONTENTS (Continued)

Page

LIST OF TABLES

Table **Page**

LIST OF FIGURES

Figure **Page**

LIST OF FIGURES(Continued)

Figure **Page**

SYMBOLS AND ABBREVIATIONS

$\dot{\varepsilon}$	=	Axial strain rate
ε	=	Strain
ε_e	=	Elastic strain
ε_p	=	Permanent strain
σ	=	Stress
E	=	Elastic modulus
η	=	Viscosity
$\varepsilon(t)$	=	Transient creep strain
$\dot{\varepsilon}(t)$	=	Steady-state creep strain rate
t	=	Time
T	=	Absolute temperature
A′	=	Empirical constant for equation (2.4 and 2.6)
B	=	Empirical constant for equation (2.4 and 2.6)
C	=	Empirical constant for equation (2.4)
B′	=	Empirical constant for equation (2.7)
n	=	Empirical constant for equation (2.7)
a	=	Strength parameters for equation (2.9)
σ_c	=	Uniaxial compressive strength
$\sigma_{c,d}$	=	Uniaxial compressive strength at dilation

SYMBOLS AND ABBREVIATIONS (Continued)

$\sigma_{c,f}$	=	Uniaxial compressive strength at failure
σ_1	=	Axial stress
$\sigma_{1,d}$	=	Axial stress at dilation
$\sigma_{1,f}$	=	Axial stress at failure
σ_3	=	Confining pressure
σ_2	=	Confining pressure
τ	=	Shear stress
S_0	=	Shear strength
μ_i	=	Coefficient of internal friction
q	=	Empirical constant for equation (2.11)
m	=	Strength parameters for equation (5.6)
$m_{,d}$	=	Strength parameters dilation
$m_{,f}$	=	Strength parameters failure
s	=	Strength parameters for equation (5.6)
c	=	Cohesion
ϕ	=	Internal friction angle
σ_n	=	Normal stress
α	=	Empirical constant for equation (5.3)
μ	=	Empirical constant to calculate β for equation (5.4 and 5.5)
W_d	=	Distortional strain energy
$W_{d,d}$	=	Distortional strain energy at dilation

SYMBOLS AND ABBREVIATIONS (Continued)

$W_{d,f}$	=	Distortional strain energy at failure
W_m	=	Mean strain energy
τ_{oct}	=	Octahedral shear stress
$\tau_{oct,d}$	=	Octahedral shear stress at dilation
$\tau_{oct,f}$	=	Octahedral shear stress at failure
γ_{oct}	=	Octahedral shear strain
$\gamma_{oct,d}$	=	Octahedral shear strain at dilation
$\gamma_{oct,f}$	=	Octahedral shear strain at failure
ε_1	=	Major Principal Strain
ε_2	=	Intermediate principal strain
ε_3	=	Minor principal strain
ε_v	=	Volumetric strain
ν	=	Poison's ratio
G	=	Shear (rigidity) modulus
λ	=	Lame′ constant
σ_m	=	Mean stress
$\sigma_{m,d}$	=	Mean stress at dilation
$\sigma_{m,f}$	=	Mean stress at failure
ε^T	=	Total strain
ε^e	=	Elastic strain
ε^c	=	Time-dependent plastic strain

SYMBOLS AND ABBREVIATIONS (Continued)

ε^{*c}	=	Equivalent creep strain
σ^{*}	=	Equivalent (effective) stress
κ	=	Material parameter
β	=	Material parameter
γ	=	Material parameter
σ_P	=	Pillar stress
$\sigma_{P,d}$	=	Pillar stress at dilation
$\sigma_{P,f}$	=	Pillar stress at failure
FS.	=	Factor of safety
e	=	Extraction ratio
H	=	Mine depth
ρ	=	In-situ stress gradient of overburden
ε_P	=	Pillar strain
ε_A	=	Axial strain
ε_L	=	Lateral strain

CHAPTER I

INTRODUCTION

1.1 Background and rationale

Time-dependent deformation (creep) of rock salt is commonly determined by subjecting salt specimen to constant deviatoric and mean stresses (ASTM D7070-08). The measured strain-time curves can be used to develop constitutive models which can range from simple rheological equations to complex visco-elastic and visco-plastic equations. The compressive strength of salt is commonly required for the design of the mine openings. It can be obtained from separated test configurations (ASTM D7012-07). Based on the standard practice the salt specimen is subjected to a constant loading rate (normally specified as 0.1 MPa/s). The salt strengths obtained under such relatively rapid loading however may not truly represent those under in-situ condition due to the fact that the mechanical responses of rock salt are sensitive to loading and strain rates (Liang et al., 2010, Fuenkajorn and Daemen, 1988, and Fuenkajorn et al., 2012). To obtain a long-term strength a wider range of loading or strain rates is required to impose on the salt specimens while monitoring the changes of the stresses and strains. The time-dependent strengths are important for the stability analysis of the salt mines and storage caverns. To ensure the long-term stability of the underground structures (e.g., supported pillars, shaft foundationsand borehole stability) the relationship between the strength, time and applied stress is needed.

1.2 Research objectives

The objective of this research is to determine the time-dependent strengths of rock salt as applied to the stability prediction of salt pillars. The effort involves performing uniaxial and triaxial compression tests on rock salt specimens under constant axial strain rates ranging from 10^{-7} to 10^{-4} s^{-1}, development of strain energy density criterion of the salt specimens, and prediction of the time-dependent dilation and failure strengths of the salt pillars.

1.3 Research methodology

The research methodology shown in Figure 1.1 comprises 7 steps; including literature review, sample preparation, uniaxial and triaxial strength testing, assessment of strength criterion, analysis and prediction and discussions and conclusions.

1.3.1 Literature review

Literature review is carried out to study the previous researches on the effect of rate on compressive strength and deformability of rock salt, salt behavior, creep model, strength criteria and stability of salt pillar. The sources of information are from text books, journals, technical reports and conference papers. A summary of the literature review is given in the thesis.

1.3.2 Sample Preparation

Rock samples used here have been obtained from the Middle members of the MahaSarakham formation in the northeastern Thailand. The rock salt is relatively pure halite. Sample preparation is carried out in the laboratory at

SuranareeUniversity of Technology. Samples prepared for compressive strength test are 54×54×108 mm^3.

1.3.3 Laboratory Testing

The laboratory testing includes uniaxial and triaxial compression tests. Axialstrain rates vary from 10^{-7}, 10^{-6}, 10^{-5} to 10^{-4} s^{-1}. A polyaxial load frame developed by Fuenkalorn et al. (2012) is used to apply confining pressures from 0, 3, 7 to 12 MPa.

The test methods and calculation follow relevant ASTM standard practices. The elasticmodulus and compressive strength are measured. Perforated neoprene sheets have been

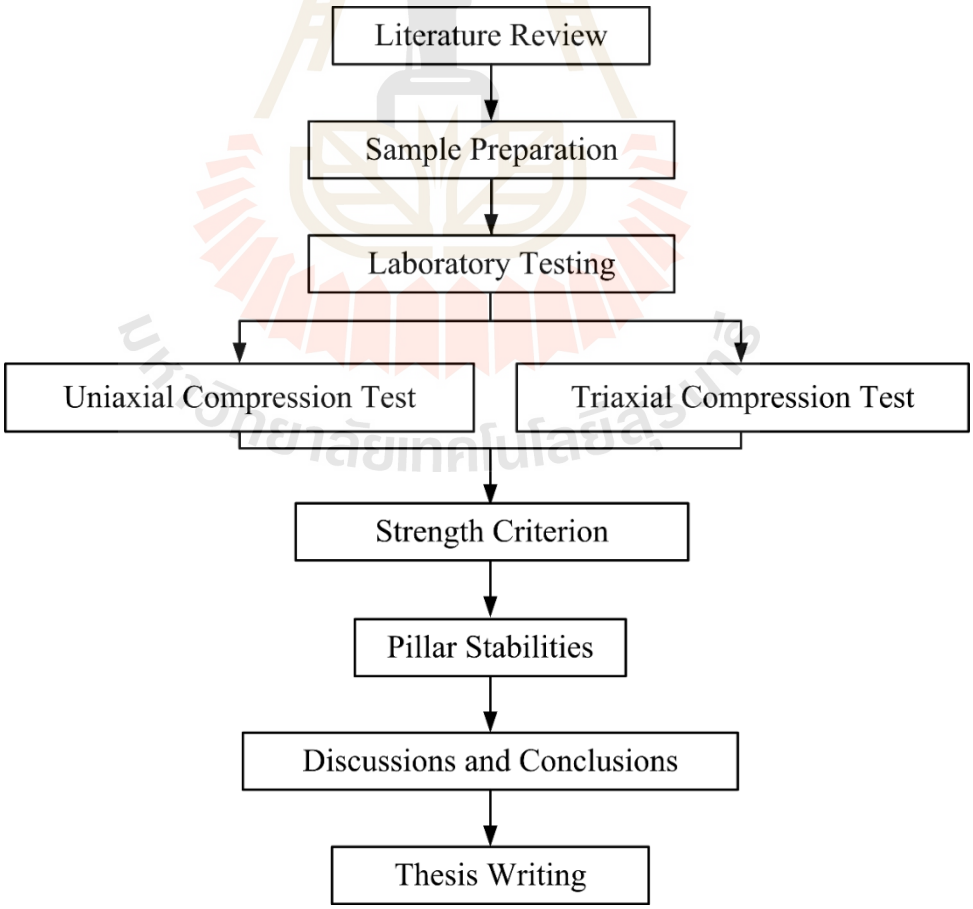

Figure 1.1 Research Methodology.

placed at the interface between loading platens and rock surfaces to minimize the friction. The loading is applied until the measured axial stress reaches the strain softening region andapproachesthe defined confining pressure. During the test, the axial stress and lateral strain are monitored. The stresses at dilation and at failure are identified.

1.3.4 Strength Criterion

Results from laboratory measurements in terms of the principal stresses at dilation and at failure and axial, lateral and volumetric strains are used to formulate mathematical relations. The studied strengthcriteria include the Coulomb, Hoek and Brown and the strain energy criteria.

1.3.5 Pillar Stabilities

The strain energy density criterion under various constant axial strain rates and confining pressureare used to develop the creep models to determine the time-dependent dilation and failure of pillar in salt mines. Governing equations for the stabilities of pillars can be derived. The research findings are described.

1.3.6 Discussions and Conclusions

Discussions and conclusionsare made on the reliability and inadequacies of the approaches used here. Future research needs are identified.

1.3.7 Thesis Writing

All research activities, methods, and results are documented and compiled in the thesis. The research or findings are published in the conference proceedings or journals.

1.4 Scope and limitations

The scope and limitations of the research include as follows.

1. All tests are conducted on rock salt specimens obtained from the Lower Salt member of the MahaSarakham formation in northeastern Thailand.
2. The salt specimens are prepared as rectangular blocks with nominal dimensions of 54×54×108 mm^3.
3. The applied axial strain rates range from 10^{-7} to 10^{-4} $s^{-1}$with the confiningpressures varying from 0, 3, 7 to 12 MPa.
4. The test procedures follow the relevant ASTM standard practices, as much as practical.
5. All tests are conducted under ambient temperature.
6. Testing is made under dry condition.

1.5 Thesis contents

Chapter I describes the background and rationale, the objectives, the methodology and scope and limitations of the research. **Chapter II** present results of the literature review on strain rate effects on salt, salt behavior, creep model, strength criteria and application. **Chapter III** describes the salt sample collection and preparation. **Chapter IV** describes the laboratory testing and test results. **Chapter V** describes the strength criteria.**Chapter VI** describes the application of this research.**Chapter VII** is the discussions, conclusions andrecommendations for future studies.

CHAPTER II

LITERATURE REVIEW

2.1 Introduction

Relevant topics and previous research results are reviewed to improve an understanding the effect of strain rate on strength and deformability of MahaSarakham salt. The effects of strain rate on salt strength and elasticity are also investigated. Initialreview results are summarized below.

2.2 Strain Rate Effect on Salt

Fuenkajorn and Deamen (1988) conducted the strain-rate controlled uniaxial test performed by loading 94 mm diameter cylinders at a constant strain rate ranging from 1×10^{-3} to 1×10^{-5} s^{-1}, and monitoring the axial stress. Four salt specimens show strain-softening, with an ultimate stress and tangent elastic modulus of 18±1.5 MPa and 25±1 GPa respectively. The constant strain rate uniaxial test is performed by axially loading a salt cylinder at a constant strain rate and recording the change in the axial stress as a function of time. The failure started developing at the midsection of the sample, as shown by chipping of small salt fragments and development of small vertical cracks (10-20 mm long) around the sample circumference. The modes of failure are similar to the first twosamples. All salt samples have an ultimate stress near 18 MPa. The strength seems to beindependent of strain rates. The stresses before peak stress

mightoverestimate the actual stress, while the stresses after the peak stress underestimatethe actual stress since the cross-sectionalarea of the samples increases due to spalling. Also they have performed triaxial testing on fifteen 57 mm diameter salt cylinders at constant strain rates and confining pressures ranging from 1×10^{-4} to 1×10^{-6} s^{-1} and from 0.3 to 7 MParespectively. At a strain rate of 4.5×10^{-5} s^{-1}, brittle-to-ductile transition pressures are 3.4-4 MPa, where salt behaves as strain-softening at strain rates higher than 2×10^{-4} s^{-1}, and as strain-hardening for rates lower than 2×10^{-5} s^{-1}. The salt samples tend to behave as a brittle (strain-softening) material when they are subjected to high strain rates (greater than 2×10^{-4} s^{-1}) and as ductile (strain-hardening) at lower strain rates (less than 2×10^{-5} s^{-1}). This could be better demonstrated if a larger range of strain rates was used. At a strain rate of 4.5×10^{-5} s^{-1}, brittle-to-ductile transition confining pressures are 3.4-4 MPa, where the salt sample behaves as a perfectly plastic material. The salt behaves as strain-hardening under confining pressures of 4.0 MPa and larger, and as strain-softening under confining pressures lower than 3.4 MPa. The transition pressure would be higher if lower strain rates were used. The sample volume tends to decrease at the beginning of loading and increase approximately after the peak stress has been reached.

Liang et al. (2011) study effect of strain rate on the mechanical properties of salt rock by uniaxial compression test under loading with $\dot{\varepsilon}$ values of 2×10^{-5}, 2×10^{-4} and 2×10^{-3} s^{-1}. Average UCS values are 13.6, 13.9, and 12.4 MPa, respectively for $\dot{\varepsilon}$ values of 2×10^{-5}, 2×10^{-4} and 2×10^{-3} s^{-1}. From the results of uniaxial compression test with different strain rates it found that the peak strength of rock salt is little affected by the strain rate (within the chosen range for $\dot{\varepsilon}$). The relationship between strain rate and strain failure of rock salt: with increasing $\dot{\varepsilon}$ value, the strain at peak strength is

less. For example, the strain-to-failure is 1.3-1.7% (specimen #1, #2) when $\dot{\varepsilon} = 2\times10^{-5}$ s^{-1}; however, it decrease to 0.3-0.7% (specimen #5, #6) when $\dot{\varepsilon}$ is increased to 2×10^{-3} s^{-1}. The rock strength of salt rock is only slightly affected by loading strain rate. The elastic modulus slightly increases with strain rate, but the increment is small. Under the same strain rate, the strength of thenardite is somewhat larger than rock salt, mainly related to crystal grain size and fabric of the minerals.

Liang et al. (2007) studied the mechanical properties of bedded salt rock. The uniaxial and triaxial compression tests are performed on rock salt (halite), interlayers (anhydrite) and bedded composite specimens (anhydrite-halite and mudstone-halite). The confining pressure is maintained constant ranging from 0, 5, 10 to 15 MPa. The applied constant strain rate is 5×10^{-5} s^{-1}. Halite begins to act viscoplastically at about σ_3~10 MPa, and this has a profound effect on the behavior of composite specimens. In the anhydrite-halite specimens, the discrepancy between the strengths of the beddedcomposite specimen and the constitutive component specimens (pure halite and anhydrite specimens) becomes less as the confined stress is increased. The effect of confining stress on Young's modulus and Poisson's ratio. These effects were attributed to sampling damage for some of the changes in stiffness response with σ_3, particularly at the lower confining stress values, and data reporting the nominal Poisson's ratio were attributed to the viscoplastic and dilatant behavior of halite at low stresses and high strain rates.

Lajtai et al. (1991) study the effect of strain rate on strength on two widely different rock types. Tyndallstone is a brittle material that deforms in an approximately elastic manner. The second rock Lanigan potash, is a ductile salt rock that has a strongly nonlinear stress-strain curve. Lanigan potash is tested for five

uniaxial compression, three confining pressures at 2 and 5 MPa. In uniaxial compression, five different strain rates were used: 0.035, 0.11, 1.75, 3 and 25 με/s. For the triaxial tests, only three rates: 0.11, 1.75 and 25 με/s were employed. The effect of the strain rate is quite large, with the slower rates causing a considerable reduction in standard triaxial strength. The data available suggest that the rate effect becomes greater with increasing confining pressure.

Dubey and Gairola (2005) study the stress-strain behavior and mechanics properties on rock salt samples collected from Guma rocksalt Mine, India. Cylindrical samples cored perpendicular to the bedding planes, were compressed using an automated closed look servo-controlled testing machine at stress rates ranging from 9.12×10^{-3} MPa/minute to 9.12 MPa/minute. The stress-strain curves obtained by compression of rock salt specimen at various stress rates exhibit similar pattern but there are distinct differences in geometry. The mechanical properties like yield stress, peak stress, compaction stress, compaction strain and failure strain in rock salt undergoing deformation by compression are stress rate dependent. The present work suggests that at very high stress rates the yield stress and peak stress could become equal and at high stress rates rock salt exhibits brittle deformation. For the lower stress rates, the peak stress is not equal to the yield stress and the rock salt deforms by viscoplastic flow. As the stress rates decrease the peak stress and yield stress decreases and compaction stress and the compaction strain increases.

Sriapai et al. (2011) studied the uniaxial and triaxial compression tests have been performed on Maha Sarakham salt to assess the influence of loading rate on the compressive strength of the rock. The salt specimens with a nominal dimension of $5.4\times5.4\times5.4$ cm^3 are compressed to failure using a polyaxial load frame. The lateral

confining pressures are maintained constant at 0, 3, 7, 12, 20 and 28 MPa while the axial stresses are applied at constant rates of 0.001, 0.01, 0.1, 1.0 and 10 MPa/s. The salt strengths exponentially increase with the loading rates. The effect is more pronounced under high confining pressures.

2.3 Salt behavior

Researchers from the field of material sciences believe that rock salt behavior shows many similarities with that of various metals and ceramics (Munson and Wawersik, 1993; Chokski and Langdon, 1991). However, because alkali halides are ionic materials, there are some important differences in their behavior. Aubertin et al. (1992, 1993, 1998, and 1999) conclude that the rock salt behavior should be brittle-to-ductile materials or elastic-plastic behavior. This also agrees with the finding by Fuenkajorn and Daemen (1988), Fokker (1995, 1998), and Fokker and Kenter (1994).

Bonding between grains can affect the creep rate and the strength of salt. The bonding between the crystals is weak in rock salt. Allemandou and Dusseault (1996) observe the post-failure from the Brazilian strength test and uniaxial compressive strength tests. They report that stress depends on the boundary between grains and crystals.

They are divided into three characteristics: the elastic, the elastic-plastic, and the plastic behaviors. The elastic behavior of rock salt is assumed to be linearly elastic with brittle failure. The rock salt is observed as linear elastic only for a low magnitude of loading. The range of linear elastic mainly depends on the content of elastic strain and can be used to formulate the modulus of elasticity. Normally, the modulus of elasticity of rock salt is relatively low. The elastic and plastic behavior of

rock salt can be investigated from the rock salt specimen. The confined rock salt specimen at the beginning of incremental loading shows linear elastic deformation but with further load increases plastic behavior is induced, which continues until yield failure. Elastic deformation and plastic deformation are considered as separated modes of deformability in the great majority of cases. The salt material simultaneously exhibits both elastic strain and plastic strain. The difference between elastic behavior and plastic behavior is that elastic deformation is temporary (recoverable) and plastic deformation is permanent (irrecoverable). The degree of permanent deformation depends on the ratio of plastic strain to total strain. The elastic and plastic deformations can also be observed by short-term loading, but at higher load magnitude. The plastic behavior of rock salt does not occur if the applied stress is less than yield stress. The rock salt is deformed continually if the high stress rate is still applied and is more than the yield stress. Increasing the load to exceed the strain limit of the rock salt beyond its strength causes it to fail. The deformation of rock salt by the increase of temperature can also result in the transition of brittle-to-ductile behavior.

The time-dependent deformation (or creep) is the process at which the rock can continue deformation without changing stress. The creep strain seldom can be recovery fully when loads are removed, thus it is largely plastic deformation. Creep deformation occurs in three different phases, as shown in Figure 2.1, which relatively represents a model of salt properties undergoing creep deformation due to the sustained constant load. Upon application of a constant force on the rock salt, an instantaneous elastic strain (ε_e) is induced. The elastic strain is followed by a primary or transient strain, shown as Region I. Region II, characterized by an almost constant

slope in the diagram, corresponds to secondary or steady state creep. Tertiary or accelerating creep leading to rather sudden failure is shown in Region III. Laboratory investigations show that removal of applied load in Region I at point L will cause the strain to fall rapidly to the M level and then asymptotically back to zero at N. The distance LM is equal to the instantaneous strain ε_e. No permanent strain is induced here. If the removal of stress takes place in the steady-state phase the permanent strain (ε_p) will occur. From the stability point of view, salt structure deformations after constant load removal have only academic significance, since the stresses imposed underground due to mining operations are irreversible. The behaviour of the salts with time-dependent deformation under constant load is characterized as a visco-elastic and visco-plastic phenomenon. Under these conditions the strain criteria are superior to the strength criteria for design purposes, because failure of most salt pillars occurs during accelerated or tertiary phase of creep, due to the almost constant applied load.

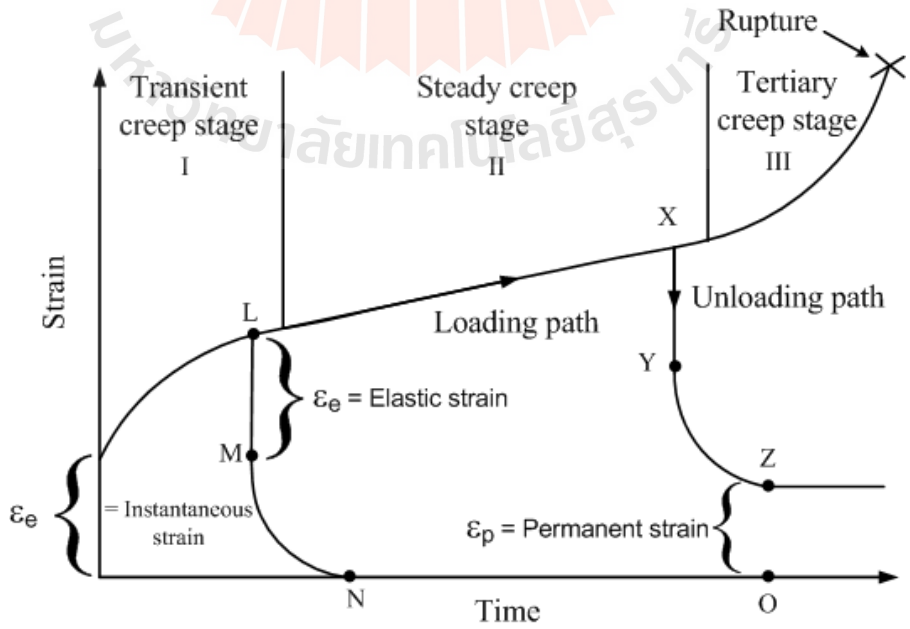

Figure 2.1 The typical deformation as a function of time of creep materials (modified from Jeramic, 1994).

The dimensions of a pillar in visco-elastic and visco-plastic rock should be established on the basis of a prediction of its long-term strain, to guard against adequate safety factor accelerating creep (Fuenkajorn and Daemen, 1988; Dusseault and Fordham, 1993; Jeremic, 1994; Knowles et al., 1998).

2.4 Creep Model

The Burgers model is one of linear visco-elastic models. These models yield a linear relationship between stress (σ) and strain rate ($\dot{\varepsilon}$) as follows:

$$\sigma+\left(\frac{\eta_1}{E_1}+\frac{\eta_2}{E_2}\frac{\eta_1}{E_2}\right)\dot{\sigma}+\frac{\eta_1\eta_2\ddot{\sigma}}{E_1E_2}=\eta_1\dot{\varepsilon}+\frac{\eta_1\eta_2\ddot{\varepsilon}}{E_2} \tag{2.1}$$

The Burgers models can describe equations for uniaxial constant stress, constant stress rate and constant rate testing. The derivation is made by using a Laplacetransformation. For uniaxial constant stress, visco-elastic are presented as function of constant axial stress (σ_0), time and spring and dashpot constant shown in Figure 2.2 and equations as follows:

$$\varepsilon(t)=\sigma_0\left\{\frac{1}{E_1}+\frac{t}{\eta_1}+\frac{1}{E_2}\left[1-\exp\left(-E_2t/\eta_2\right)\right]\right\} \tag{2.2}$$

Langer (1984) and Farmer (1983) presented numerous empirical equations describing the time-dependent behavior of geological materials. Two types of empirical laws that explicitly contain creep strain, stress, and time variables are

selected for use this investigation potential laws and exponential laws. The laws are applied to describe salt behavior without considering the actual mechanism of deformation. Generally, empirical constitutive model are developed by linking the creep strain to stress and temperature. The potential laws are power equations relating creep strain, stress, time and temperature. Two empirical models describing transient and steady-state creep strains can be expressed as:

$$\varepsilon(t) = K'\sigma^{\beta} t^{\gamma} T^{\alpha} \qquad \text{(transient)} \qquad (2.3)$$

$$\dot{\varepsilon}(t) = A'\sigma^{B} T^{C} \qquad \text{(steady-state)} \qquad (2.4)$$

For the isothermal condition, the equation reduce to:

$$\varepsilon(t) = K'\sigma^{\beta} t^{\gamma} \qquad \text{(transient)} \qquad (2.5)$$

$$\dot{\varepsilon}(t) = A'\sigma^{B} \qquad \text{(steady-state)} \qquad (2.6)$$

The exponential laws present the transient creep strain as a function of stress, time and temperature in exponential form:

$$\varepsilon(t) = B'\sigma^{m} t^{n} \exp(-\lambda/T) \qquad (2.7)$$

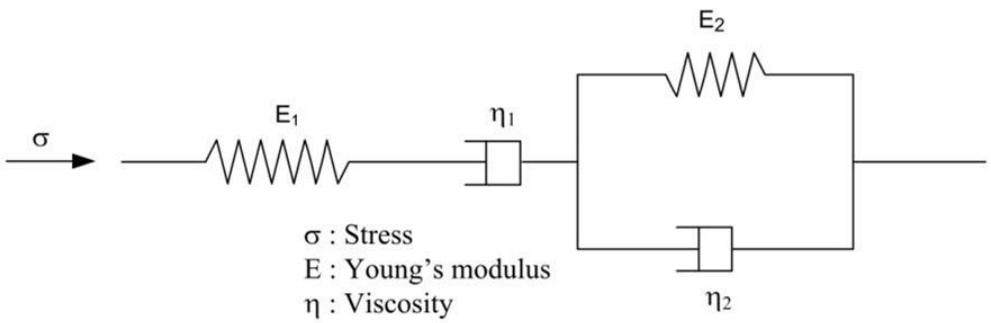

Figure 2.2 Burger model built up of combination of linear spring and dashpots.

where$\varepsilon(t)$ is transient creep strain, $\dot{\varepsilon}(t)$ is steady-state creep strain rate, σ is stress, t is time, T is absolute temperature andκ', α, β, γ, A′, B, C, B′, m, n, $\lambda$are empirical constants.

2.5 Strength Criteria

The Hoek-Brown (1980) criterion defines the relationship between the major and minor principal stresses at failure as:

$$\sigma_1 = \sigma_3 + \sqrt{m\sigma_C\sigma_3 + s\sigma_C^2} \tag{2.8}$$

where σ_1 and σ_3 are the effective major and minor principal stresses, respectively, at failure; σ_C is the uniaxial compressive strength of the intact rock; m, s and a are the strength parameters depending on the quality of the rock mass, and can be estimated by empirical expressions involving the geological strength index (GSI) and disturbance factor. Moreover, the original form of intact rock material (i.e. s = 1 and a = 0.5) has not been changed and is given by Hoek et al. (2002) propose a generalized form of the Hoek-Brown criterion as:

$$\sigma_1 = \sigma_3 + (m\sigma_C\sigma_3 + s\sigma_C^2)^a \tag{2.9}$$

where m is the Hoek-Brown parameter for intact rock material. The parameter m is dimensionless, and its value is affected by inter-particle friction and the degree of

particle interlocking. Although it has been noted that Eq. 2.9 is applicable to isotropic rocks, it may be modified to predict the failure of anisotropic intact rocks.

Coulomb criterion indicates that when shear failure takes place across a plane, the normal stress σ_n and the shear stress τ across this plane are related by functional relation characteristics of the material (Jaeger et al., 2007):

$$|\tau| = S_0 + \mu_i \sigma_n \tag{2.10}$$

where S_0 is the shear strength or cohesion of the material and μ_i is the coefficient of internal friction of the material. Since the sign of τ only affects the sliding direction, only the magnitude of τ matters. The linearzed form of the Mohr failure criterion may also be written as (Jaeger et al., 2007):

$$\sigma_1 = \sigma_C + q\sigma_3 \tag{2.11}$$

where: $q = \left[\left(\mu_i^2 + 1\right)^{1/2} + \mu_i^2\right]^2 = \tan^2\left(\pi/4 + \phi/2\right)$

where σ_1 is the major principal effective stress at failure, σ_3 is the least principal effective stress at failure, σ_c is the uniaxial compressive strength and ϕ is the internalfriction angle equivalent to $\tan^{-1}\ \mu_i$. This failure criterion assumes that the intermediate principal stress has no influence on failure.

Sriapai et al. (2012) used the strain energy density criterion to describe the salt strength and deformability under different temperatures. It is assumed that under a given mean strain energy and temperature the distortional strain energy required to fail the salt specimens is constant. Regression on the test results shows that the distortional strain energy (W_d) increases linearly with the mean strain energy (W_m). It

is interesting to note that the rates of the increase of W_d with respect to W_m are virtually the same for all temperature levels.

Fuenkajorn et al. (2012) were proposed empirical strength criteria base on the strain energy density principle of rock salt. Uniaxial and triaxial compression tests have been performed to assess the influence of loading rate on the compressive strength and deformability of the Maha Sarakham alt. The salt specimens with a nominal dimension of 5.4×5.4×5.4 cm^3 are compressed to failure using a polyaxial load frame. The lateral confining pressures are maintained constant at 0, 3, 7, 12, 20 and 28 MPa while the axial stresses are increased at constant rates of 0.001, 0.01, 0.1, 1.0 and 10 MPa/s until failure occurs. The salt elasticity and strength increase with the loading rates. The elastic (tangent) modulus determined at about 40% of the failure stress varies from 15 to 25 GPa, and the Poisson's ratio from 0.23 to 0.43. The elastic parameters tend to be independent of the confining pressures. The strains induced at failure decrease as the loading rate increases. Various multiaxial formulations of loading rate dependent strength and deformability are derived. The variation of the octahedral shear stresses and strains induced at dilation and at failure with the applied shear stress rates can be best described by power relations. The distortional strain energy at dilation and at failure from various loading rates varies linearly with the mean normal stress. The proposed empirical criteria are applied to determine the safe maximum withdrawal rate of a compressed-air energy storage cavern in the Maha Sarakham salt formation. The strain energy criterion that considers both distortional and mean stress-strains at dilation tends to give the most conservative results.

Artkhonghan (2015) proposed energy criterion derived from constant mean stress data, which tends to give the most conservative results. The strain energy

density assumes that the stress-strain relations are linear. In reality, however, non-linear behavior has been observed for all test conditions and stress paths, in particular for the salt under large σ_3 and σ_m. As a result the strain energy determined here likely underestimates the energy that the in-situ salt can sustain before failure. This makes the application of the strain energy criterion to the stability evaluation even more conservative. The advantage of the application of the strain energy criterion over the traditional strength criteria is that it considers both shear stress and strain at failure, and hence their results would be more comprehensive than the modified Wiebols and Cook and Mogi criteria, particularly for soft and creeping rocks, such as salt, where their strains at failure are large.

Sartkaew and Fuenkajorn (2013) have been performed the uniaxial compression test to assess the effects of loading rate on compressive strength and deformability of the Maha Sarakham salt under temperatures ranging from 273 to 373 Kelvin. The variation of the octahedral shear strength with the stress rates and temperatures can be described by logarithmic relations. The distortion strain energy criterion is proposed to describe the salt strength under varied stress rates and temperatures. The criterion can be used to determine the stability of salt around compressed-air energy storage caverns, where the loading rates and temperatures are continuously varied during air injection and retrieval periods.The testing is assumed to be under isothermal conditions (constant temperature with time during loading). The decrease of the salt strength as the temperature increases suggests that the applied thermal energy before the mechanical testing makes the salt weaker, and more plastic, failing at lower stress and higher strain with lower elastic and shear moduli.

2.6 Pillar Stabilities

Hyder et al. (2011) propose simulation and modeling of pillar stability and analysis of safety factor. The material properties assigned to the model are obtained by testing the representative samples taken from the selected locations of the mine. The mine under investigation has 50 ft wide pillars and 50 ft wide rooms under an average overburden of 650 feet. The effect of reduced pillar dimensions and increased roof span on overall stability of mine and extraction ratio is analyzed using LaModel software. The mine consists of many thousands of such section so it is a huge recovery of salt. The modeling can provide the basis for actual mine implementation of this model and optimum resource utilization can be achieved efficiently. The mechanical properties were determined in the rock mechanics laboratory on the representative samples of salt. The following mechanical properties were determined.

- Uniaxial compressive strength
- Poisson's ratio
- Modulus of elasticity
- Tensile strength

The study finds that the pillars have excessively large dimensions and large quantities of salt can be recovered by pillar reductions without affecting the safety of mine and operations. The result indicates that by reducing the size of pillars from 50 ft×100 ft×16 ft to 30 ft×80 ft×16 ft, 117, 363 metric tons of salt can be recovered from the section understudy, comprising of a series of 5×10 pillars. This modeling can provide

the basis for actual mine implementation of this model and optimum resource utilization can be achieved efficiently. They was found that the present practice of having 50 ft wide pillars and 50 ft wide rooms irrespective of overburden depth and other relevant factors was unnecessarily resulting in low extraction ratio, so it should be revised to optimize the size of pillar and roof span to get better extraction ratio without compromising safety.

Lau (2010) explain the convergence rate decreased as the pillar width to pillar height ratio increased. In addition, the convergence rate began to stabilize for salt thicknesses larger than 15 m for the modeled pillar width to pillar height ratios. This is due to the limitations of the stress bulb, where the overbearing capacity affects the stress in the underlying material until a certain depth. Vertical and horizontal stresses were also observed to verify the modeled results reflected actual room and pillar behavior in salt mines. After simulating the model for 20 years, the vertical stresses were the largest in the center of the pillar and near zero at the edges of the pillar. The convergence rate and the pillar width to pillar height ratio exhibited an exponential relationship for all modeled pillar width to pillar height ratios, which was used as the base for the developed relationship between convergence rate and pillar width to pillar height ratio. The convergence rate found from modeling and the convergence rate calculated from the developed relationship showed a strong correlation. The average percentage error between the modeled results and the calculated results was 5.92% for all of the simulations. The percentage error was higher for salt thicknesses larger than 10 m.

Sambeek (1997) used the finite element method to determine the pillar strain rates and room closure rates or deformation rates for various pillar width to pillar

eight ratios. The purpose was to validate the pillar design equations by comparing the results of the equations with modeling results. The pillar height and extraction ratio was kept constant. Pillar width to pillar height ratios of one to five was used in the modeling. Van proposed the average horizontal stress and the average vertical stress are related by 10 percent of the pillar with to pillar height ratio. When determining equations to predict the average effective stress, it was found that as the pillar width to pillar height ratio becomes large, the effective stress approaches zero rapidly. Also, plane strain conditions are approached when pillars are long in one dimension. When using the equations developed by Van Sambeek for determining pillar creep rates, it was found that the pillar compression rate for rectangular pillars is 50 percent less than a square pillar with the same width, pillar height, and extraction ratio.

CHAPTER III

SAMPLE PREPARATION

3.1 Sample preparation

This chapter describes sample preparation and specifications of the tested rock salt. The method follows as much as practical the standard practices. The salt specimens tested here are obtained from salt block of ASEAN Potash Chaiyaphum Public Company Limited, Chaiyaphum province. They are from the Lower members of the Maha Sarakham formation in the northeastern Thailand. This salt member has long been considered as ahost rock for compressed-air energy storage by the Thai Department of Energy. The specimens are dry cut and ground as shown in Figure 3.1. The salt specimens are prepared as rectangular blocks with nominal dimensions of 54×54×108 mm^3 as shown in Figure 3.2. The rock salt is relatively pure halite with slight amount (less than 1-2%) of anhydrite, clay minerals and ferrous oxide. Warren (1999) gives detailed descriptions of the salt and geology of the basin. Sample preparation is conducted in laboratory facility at the Suranaree University of Technology. A total of 16 specimens are prepared for testing. Table 3.1 summarizes the specimen number, dimensions and density.

Figure 3.1 A salt specimen is dry cut by a cutting machine.

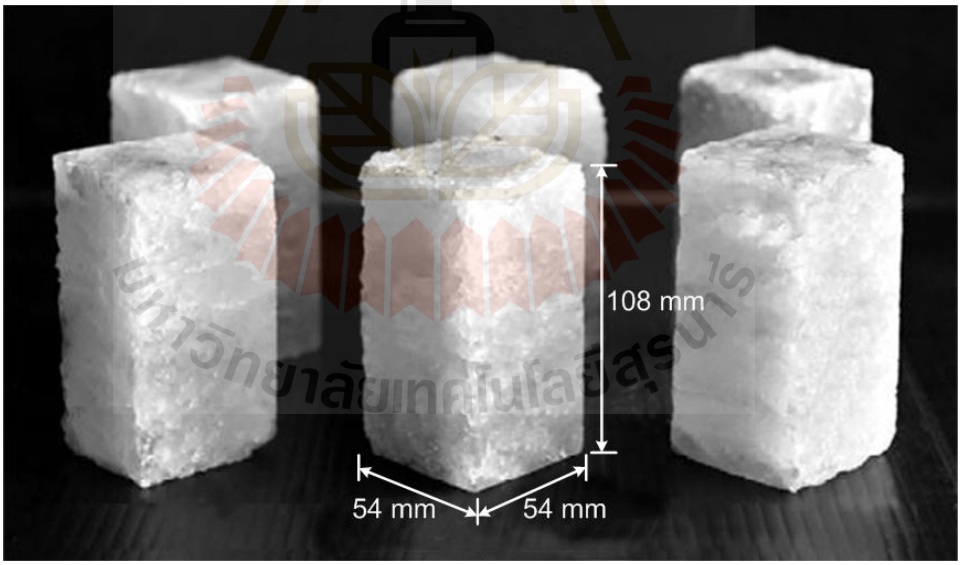

Figure 3.2 Some rectangular block specimens of salt used in the uniaxial and triaxialtesting.

Table 3.1 Salt specimens prepared for uniaxial and triaxial compression tests.

Specimen No.	Width (mm.)	Length (mm.)	Height (mm.)	Density (g/cc)
LS-TRI-01	53.63	53.16	103.94	2.12
LS-TRI-02	54.43	54.56	108.00	2.12
LS-TRI-03	52.94	54.14	107.51	2.14
LS-TRI-04	53.93	53.85	107.75	2.12
LS-TRI-05	53.78	53.49	108.20	2.11
LS-TRI-06	51.70	53.80	108.13	2.18
LS-TRI-07	53.83	52.80	109.03	2.13
LS-TRI-08	53.88	54.23	108.45	2.11
LS-TRI-09	55.30	54.55	111.43	2.11
LS-TRI-10	54.18	54.53	108.43	2.10
LS-TRI-11	54.38	54.28	107.50	2.09
LS-TRI-12	54.65	55.05	107.30	2.08
LS-TRI-13	54.40	54.95	108.18	2.10
LS-TRI-14	54.00	54.28	107.68	2.10
LS-TRI-15	54.60	54.55	110.18	2.13
LS-TRI-16	55.05	54.15	106.33	2.10

CHAPTER IV

LABORATORY TESTING

4.1 Introduction

The objective of the laboratory testing is to assess the effects of strain rate on compressive strength and deformability of the MahaSarakham salt. This chapter describesthe method and results of the laboratory experiments. The tests are divided into two groups; uniaxial and triaxial compression tests. The results have been studied to determinethe effects of strain rate effects on compressive strength and deformation properties of rock salt. The results obtained have are also compared with other researches. A total of 16 specimens have been tested.

4.2 Uniaxial compression test

The objective of the uniaxial compression tests is to determine the ultimate strength and the deformability under uniaxial load at various strain rates. The test procedures follow the American Society for Testing and Materials (ASTM D 7012-07) and the suggested methods by ISRM (Bieniawski and Bernede, 1978). The tests are performed by applying uniform axial stress under constant rate to the rectangular rock specimen and measuring the increase of axial stress and lateral strain as a function of time (Figure 4.1). The specimens areloadedfailure under strain rates varying from 10^{-7}, 10^{-6}, 10^{-5} to 10^{-4} s^{-1}.The failure stresses and lateral strains are recorded.

4.3 Triaxial compression tests

The test are conducted using a polyaxial load frame (Figure 4.2)apply constant anduniform lateral stresses (confining pressures) to the rock specimens while the axial strain is increased at a constant rate until failure occurs and continue to softening behavior. Exhaustive reviews of the polyaxial load frame have recently been given in Fuenkajorn et al. (2012). The testing system is always calibrated before testing. In this study, theconfining pressure (σ_2 and σ_3) are equal ranging from 3, 7 to 12 MPa, and the constant axial strain rates from 10^{-7}, 10^{-6}, 10^{-5} to 10^{-4} s^{-1}. Perforated neoprene sheets are used to minimize the friction at all interfaces between the loading platen and the rock surface. After installing the rectangular specimen into the load frame, dead weights are placed onthe steel bar to obtain the pre-defined magnitude of the uniform confining pressure (σ_3) on the specimen. The test is started by increasing the vertical

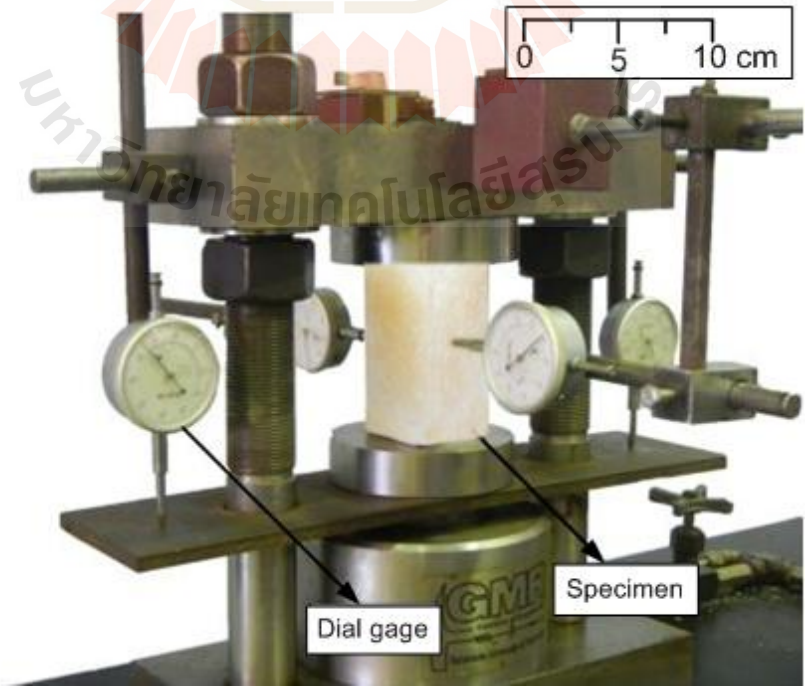

Figure 4.1 Salt specimen placed under uniaxial load frame.

stress at the predefined rate using the hydraulic pump. Both the axial strain and lateral strain were properly recorded directly by a dial gage during the testing. The failure stresses and lateral strains are recorded.

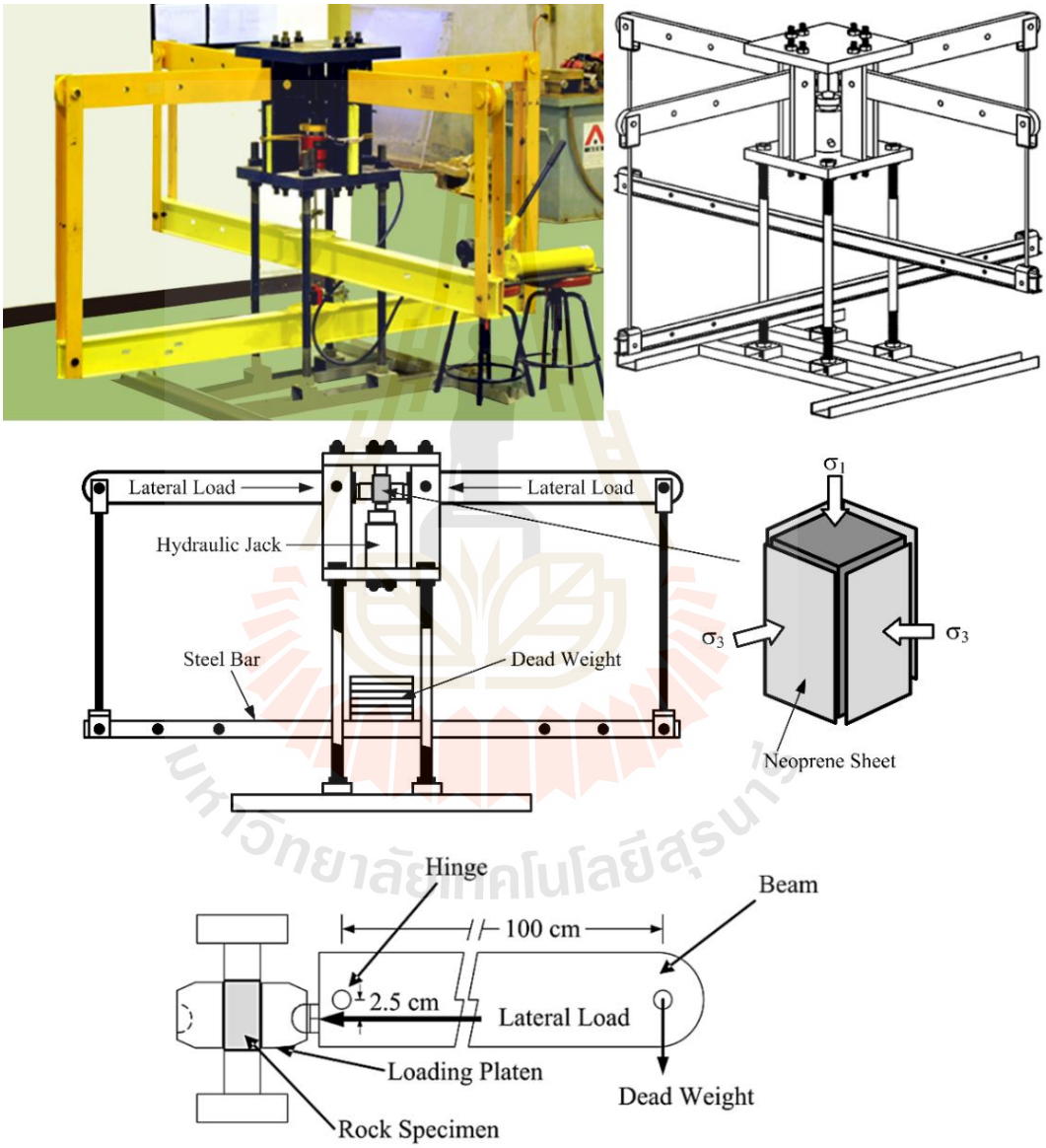

Figure 4.2 Polyaxial load frame used in this study (Fuenkajorn et al., 2012).

4.4 Test results

This section describes test results in terms of strength and elasticity. The measured sample deformations are used to determine the stress along the principal axes during loading. The axial stress and lateral and volumetric strains are measured.

4.4.1 Strength results

The uniaxial compressive strengths (σ_c) as a function of axial strain rates at dilation and at failure are shown in Figure 4.3. The dilation strength is the point at which the specimen is loaded and deformed to its elastic limit. Beyond this point the micro-cracks are initiated, the specimen volume increases, and the axial stress-strain relation is no longer linear. The results showthat the strengths at dilation ($\sigma_{c,d}$) and at failure ($\sigma_{c,f}$)logarithmically increase with increasing axial strain rate ($\dot{\varepsilon}$), and can be represented by:

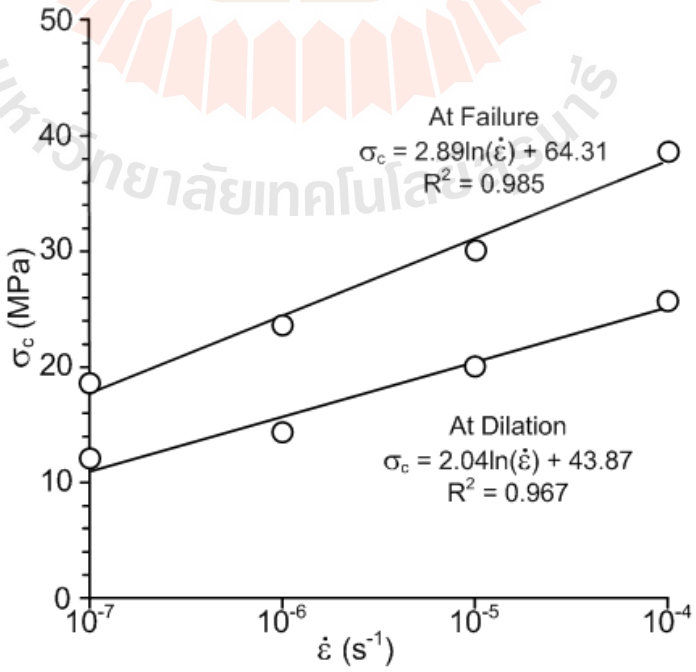

Figure 4.3 Uniaxial compressive strengths as a function of axial strain rates ($\dot{\varepsilon}$).

$$\sigma_{c,d} = 2.04\ln(\dot{\varepsilon}) + 43.871 \quad (4.1)$$

$$\sigma_{c,f} = 2.89\ln(\dot{\varepsilon}) + 64.31 \quad (4.2)$$

The exponential equations above fit relatively well to the strength results ($R^2 \geq 0.9$). The dilation strength is about 40% of the failure strength for rock salt specimens.

For triaxial compression testing, the constant and uniform lateral stresses ($\sigma_2=\sigma_3$) range from 3, 7 to 12 MPa. The specimen deformations are monitored along the three loading directions and are used to calculate the principal strains during loading. Figure 4.4 shows the measured vertical stresses as a function of axial, lateral and volumetric strain for salt under different axial strain rates and all confining pressures (0, 3, 7 to 12 MPa). The specimens tend to show nonlinear behavior, particularly under low axial strain rates. The specimens loaded under high axial strain rates ($\dot{\varepsilon}$), show higher peak stress (σ_1) than those under lower axial strain rates. Under the same axial strain rate the compressive strength (σ_1) increases with increasing confining pressures (σ_3). Similar testing results have been observed by Liang et al. (2010), Fuenkajorn and Daemen (1988) and Fuenkajorn et al. (2012). The salt strengths obtained under such relatively rapid loading however may not truly represent those under in-situ condition due to the fact that the mechanical responses of rock salt are sensitive to loading and axial strain rates.

The octahedral shear stresses (τ_{oct}) and shears trains (γ_{oct}) at failure are also determined using the following relations (Jaeger et al., 2007):

$$\tau_{oct}=(1/3)\cdot[(\sigma_1-\sigma_2)^2+(\sigma_2-\sigma_3)^2+(\sigma_3-\sigma_1)^2]^{1/2} \quad (4.3)$$

$$\gamma_{oct}=(1/3)\cdot[(\varepsilon_1-\varepsilon_2)^2+(\varepsilon_2-\varepsilon_3)^2+(\varepsilon_3-\varepsilon_1)^2]^{1/2} \quad (4.4)$$

where σ_1,σ_2 andσ_3 are the major and minor principal (when $\sigma_2=\sigma_3$) stresses andε_1,ε_2 and$\varepsilon_3$are the major, intermediate and minor principal strains.

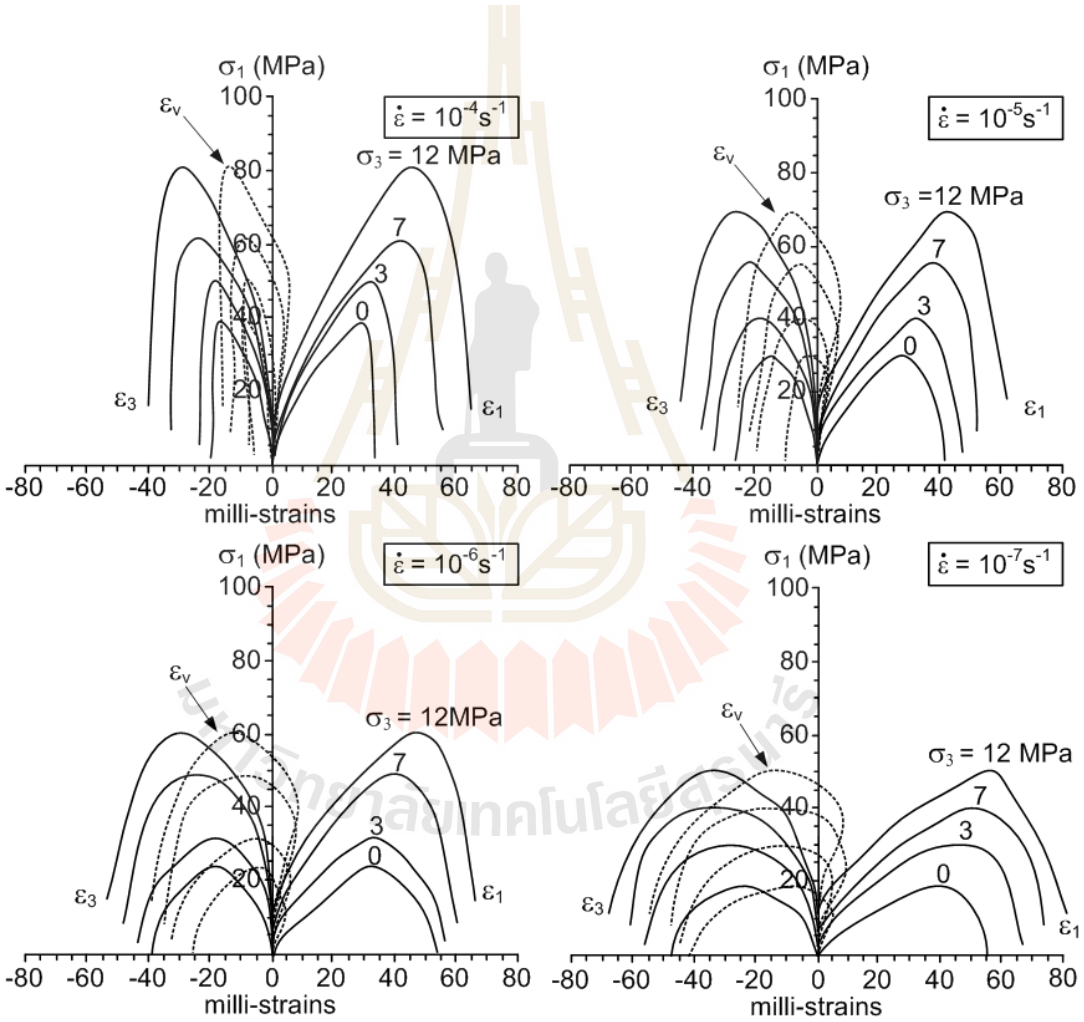

Figure 4.4 Axial stress (σ_1) as a function of axial (ε_1), lateral (ε_3) and volumetric (ε_v) strains for various confining pressures (σ_3) and strain rates ($\dot{\varepsilon}$).

To show the effects of strain rate on the salt strength and deformability the applied octahedral shear stresses are plotted as a function of octahedral shear strainin Figure 4.5.Higher strain rates applied result in higher shear strengths and lower shear strains at failure. The effects of the strain rate on the salt strength become larger under higher confining pressures.

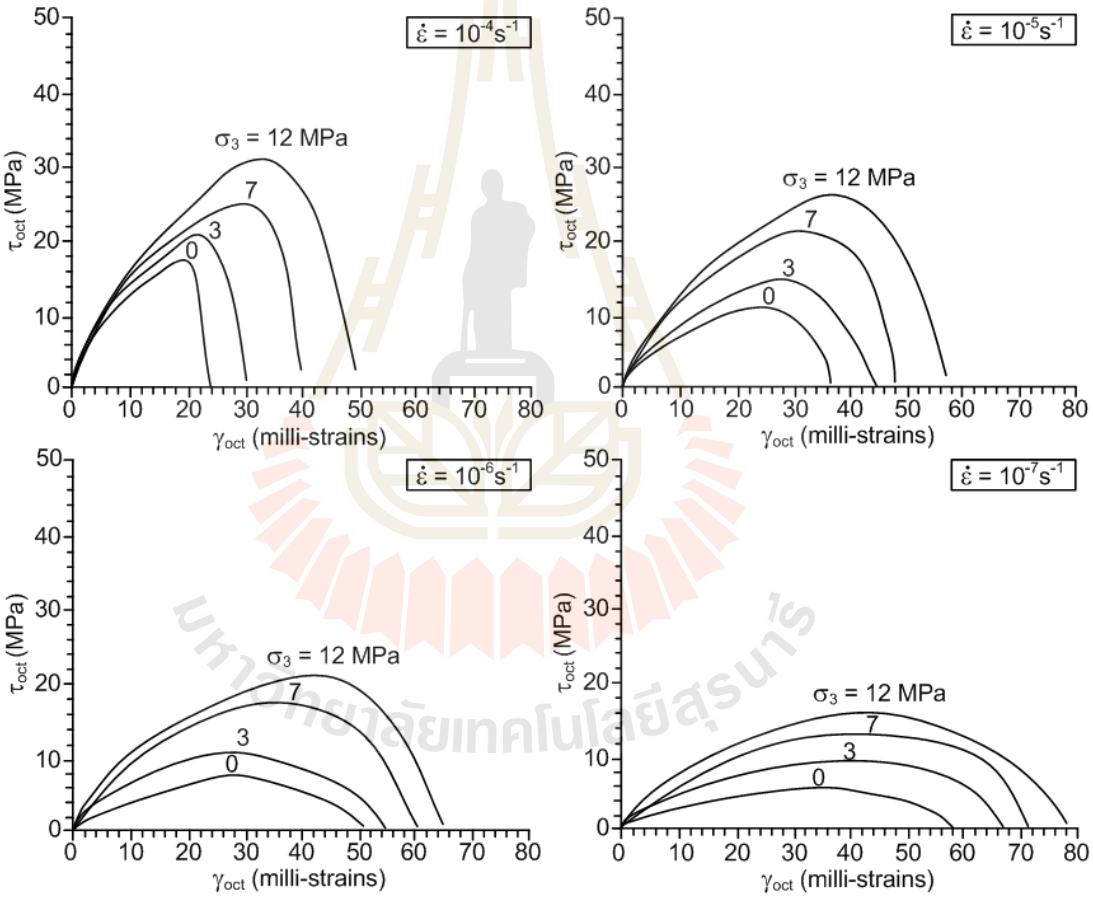

Figure 4.5 Octahedral shear stress (τ_{oct}) as a function of octahedral shear strain (γ_{oct}) for various confining (σ_3) and axial strain rates ($\dot{\varepsilon}$).

4.4.2 Elastic parameter

The elastic modulus (E) and Poisson's ratio (ν) are determined from the three-dimensional stress-strain relations where the axial and lateral stresses and strains at dilation are taken from the diagrams shown in Figure 4.4. The dilation strength is determined as the point where the specimen volume starts increasing. Assuming that the specimens are isotropic, the shear (rigidity) modulus (G), Lame′ constant (λ), and Poisson's ratio (ν) can be calculated from the following relations (Jaeger and Cook (1979)):

$$G = (1/2)\cdot(\tau_{oct}/\gamma_{oct}) \tag{4.5}$$

$$3\sigma_m=(3\lambda+ 2G)\cdot\varepsilon_v \tag{4.6}$$

$$\nu= (\lambda/2)\cdot(\lambda+ G) \tag{4.7}$$

$$E=2G\cdot(1+ \nu) \tag{4.8}$$

whereσ_m and ε_v are the mean stress, and volumetric strain at dilation (the point where the elastic parameters are determined).

The calculations of elastic parameter are made at the dilation strength. The dilation strength is determined as the point where the specimen volume starts increasing. The salt elastic moduli increase linearly with strain rate (Figure 4.6(a)):

$$E = 0.227\ln(\dot{\varepsilon}) + 4.422 \tag{4.9}$$

And the decrease of the Poisson's ratio with increasing axial strain rate can be represented by this equation (Figure 4.6(b)):

$$\nu = -0.008\ln(\dot{\varepsilon}) + 0.274 \quad (4.10)$$

Good correlations between the equations above with the test data are obtained.Table 4.1 gives the dilation and failure strengths and elastic parameter for each axial strain rate and confining pressure.

Table 4.2 summarizes some laboratory-determined mechanical properties. One distinct implication is that the mechanical properties of MahaSarakham salt tend to have high variations. These variations may be caused by internal (intrinsic) factors (i.e., differences in grain sizes, inclusion contents, and cohesive forces between grains), and by external factors (differences in specimen sizes, loading rate, stress-paths, and testing temperature). These uncertainties have raised a question about the representation and

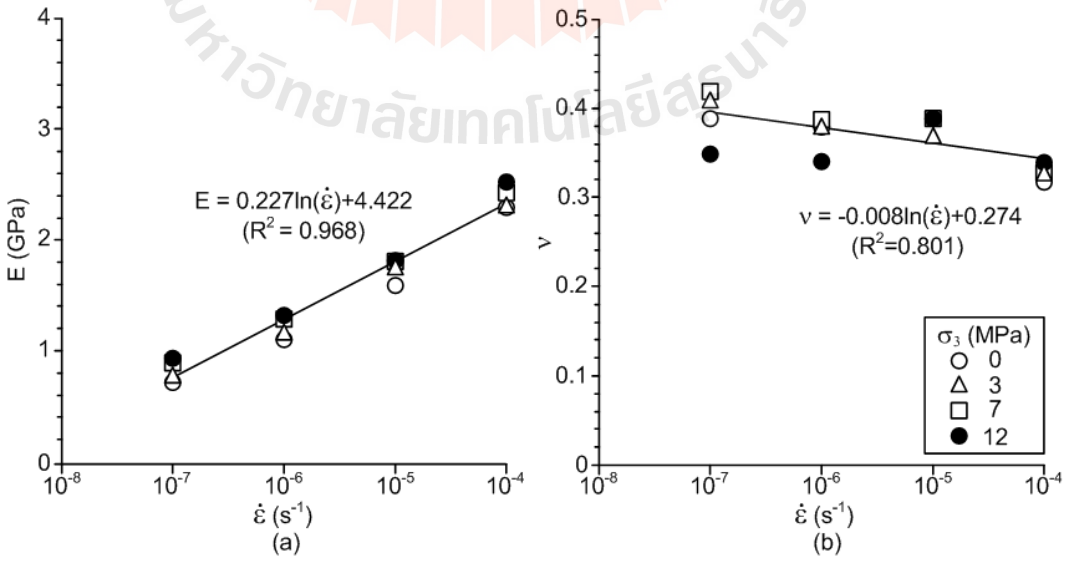

Figure 4.6 Elastic parameters obtained from uniaxial and triaxial testing.

reliability of laboratory determined properties when applied to the design and analyses of engineering structures in salt mass.

Table 4.1 Summary of the strength results on salt specimen at dilation and at failure under various strain rates.

$\dot{\varepsilon}$ (s^{-1})	σ_3 (MPa)	$\sigma_{1,d}$ (MPa)	$\sigma_{1,f}$ (MPa)	$\tau_{oct,d}$(MPa)	$\tau_{oct,f}$(MPa)	$\gamma_{oct,d}$ (10^{-3})	$\gamma_{oct,f}$ (10^{-3})	E (GPa)	ν
10^{-4}	0	17.61	38.67	12.15	18.23	8.43	19.55	2.29	0.32
	3	28.28	49.12	13.37	21.74	8.72	22.70	2.31	0.33
	7	40.96	62.92	16.01	26.36	10.44	29.03	2.42	0.33
	12	53.10	80.59	19.38	32.33	12.96	32.88	2.53	0.34
10^{-5}	0	15.19	30.03	9.46	14.15	11.14	23.24	1.59	0.39
	3	24.74	40.10	11.38	17.49	12.09	27.42	1.76	0.37
	7	37.29	55.38	15.52	22.81	3.00	32.48	1.81	0.39
	12	48.52	69.88	18.58	27.28	17.24	36.08	1.82	0.39
10^{-6}	0	12.07	23.68	6.72	11.16	12.50	26.91	1.10	0.38
	3	23.80	33.26	10.48	14.26	14.08	29.01	1.17	0.38
	7	34.56	48.29	14.25	19.46	16.78	35.88	1.29	0.39
	12	44.80	61.65	16.00	23.40	18.77	41.24	1.32	0.34
10^{-7}	0	11.30	18.64	5.70	8.78	14.25	34.22	0.72	0.39
	3	21.27	30.97	5.88	13.18	16.00	39.84	0.78	0.41

	7	28.95	40.89	10.93	15.98	17.26	41.29	0.88	0.42
	12	39.47	50.13	13.13	17.97	20.37	45.97	0.90	0.35

Table 4.2 Published mechanical properties of MahaSarakham salt.

Testing	Salt Member	σ_C (MPa)	E (GPa)	ν
Uniaxial compression test Luangthip et al. (2016)	Lower salt	39.5-69.1	16.89-22	0.27-0.31
Uniaxial and triaxial compression test Thongprapha et al. (2016)	Lower salt	37±2.5	9-24	0.37±0.48
Uniaxial and triaxial compression test Fuenkajorn et al. (2012)	Middle salt	16.5-119.7	15-25	0.23-0.43
Uniaxial and triaxial compression test Sriapai et al. (2010)	Middle salt	23-106.4	22.2±2.74	0.37±0.05
Uniaxial and temperature Sartkaew (2013)	Lower salt	29.19-37.23	20.31-24.06	0.31-0.42

CHAPTER V

STRENGTH CRITERIA

5.1 Introduction

This chapter describes the strength analysis at dilation and at failure under differentaxial strain rates. The strength criteria used in this study include the Coulomb, Hoek and Brown and the strain energy density criteria. Representativeness of these criteria can be discussed.

5.2 Coulomb criterion

Based on the Coulomb strength criterion the cohesion (c) and internal friction angle (ϕ) of the salt can be determined in terms of the principal stresses at dilation and at failure and the uniaxial compressive strength (σ_c) which can be written as:

$$\sigma_1 = \sigma_c + \sigma_3 \tan 2\phi \quad (5.1)$$

$$c = \sigma_c/(2\tan\phi) \quad (5.2)$$

$$\phi = 2\alpha - (\pi/2) \quad (5.3)$$

The cohesion and friction angle of intact salt can be obtained from regression analyses of the uniaxial compressive strength and a set of major (σ_1) and minor (σ_3)principal

stresses at dilation and at failure obtained under the same strain rate. It's found that the regression results show good correlations (R^2>0.9) between the criterion and the testdata. The parameter α is then used to calculate the cohesion and friction angle by using Eqs. (5.2) and (5.3). The c and ϕ values for each strain rate are summarized in Table 5.1, and are plotted as a function of strain rate in Figure 5.1. The cohesions tend to increase with strain rate, particularly for the peak strength. The internal friction angles however tend to be independent of the strain rate. The shear strength (τ) and normal stress (σ_n) can also be represented by:

$$\tau = (1/2)\cdot(\sigma_1 - \sigma_3)\sin 2\beta \tag{5.4}$$

$$\sigma_n = (1/2)\cdot(\sigma_1 + \sigma_3) + (1/2)\cdot(\sigma_1 + \sigma_3)\cdot\cos 2\beta \tag{5.5}$$

where $\beta = (\pi/2) - (\tan^{-1}/2\mu)$ and $\mu = \tan\phi$. Figure 5.2 compares the Coulomb criterion predictions with the test data at dilation and at failure.

Table 5.1 Cohesions and friction angles at dilation and at failure for each axial strain rate.

Strength	**$\dot{\varepsilon}$ (s^{-1})**	**c (MPa)**	**ϕ (Degrees)**
At dilation	10^{-4}	2.69	12.6
	10^{-5}	2.27	12.6
	10^{-6}	1.84	12.6
	10^{-7}	1.42	12.6
At failure	10^{-4}	11.21	31.2
	10^{-5}	9.09	31.2
	10^{-6}	6.98	31.2
	10^{-7}	4.86	31.2

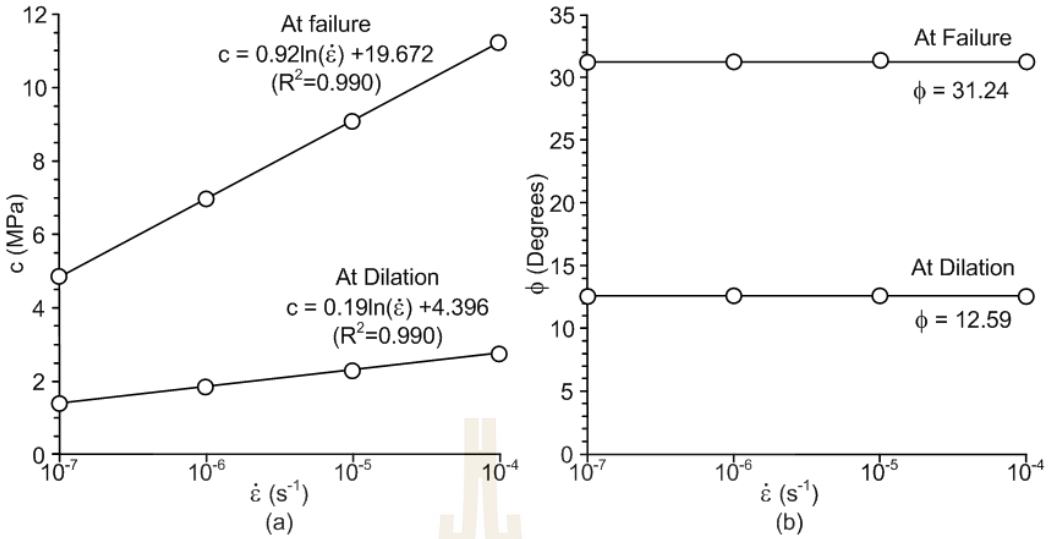

Figure 5.1 Cohesion, c (a) and internal friction angel, ϕ (b) as a function of axial strainrate ($\dot{\varepsilon}$).

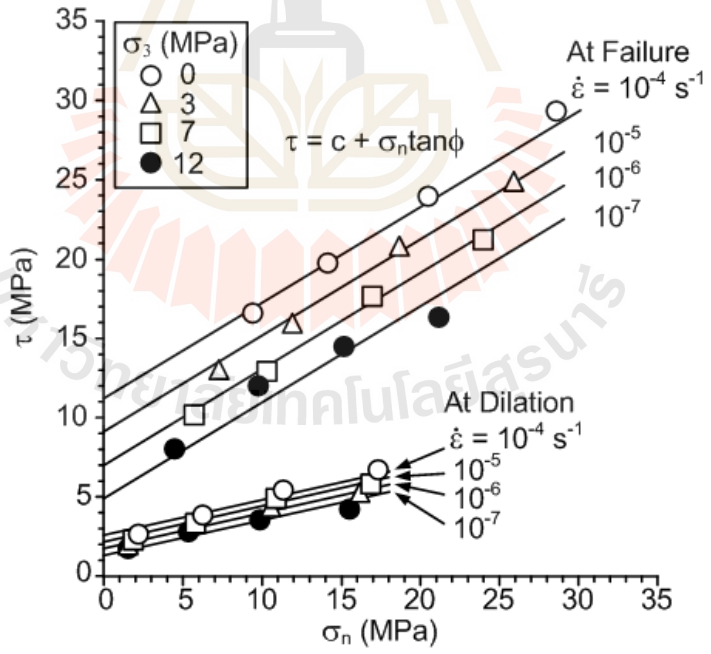

Figure 5.2 Shear strength (τ) as a function of normal stress (σ_n) for various axial strainrates ($\dot{\varepsilon}$).

5.3 Hoek and Brown criterion

The Hoek-Brown strength criterion (Hoek and Brown, 1980) is used here to describe the relationship between the major (σ_1) and minor (σ_3) principal stresses at dilation and at failure of the triaxial test results:

$$\sigma_1 = \sigma_3 + (m \cdot \sigma_3 \cdot \sigma_c + s\sigma_c^2)^{1/2} \quad (5.6)$$

where m and s are material parameters. For intact specimens used in this study, s = 1.

The criterion can be rewritten as function of principal stresses at dilation and at failure:

$$\sigma_{1,d} = \sigma_3 + (m_f \cdot \sigma_3 \cdot \sigma_{c,f} + s\sigma_{c,f}^2)^{1/2} \quad (5.7)$$

$$\sigma_{1,f} = \sigma_3 + (m_d \cdot \sigma_3 \cdot \sigma_{c,d} + s\sigma_{c,d}^2)^{1/2} \quad (5.8)$$

where m_d and m_f represent the conditions at dilation and at failure. Via regression analysis they can be defined as a function of axial strain rates ($\dot{\varepsilon}$) as:

$$m_d = -0.0002(\dot{\varepsilon}) + 6.52 \quad (5.9)$$

$$m_f = 0.00001(\dot{\varepsilon}) + 4.40 \quad (5.10)$$

By substituting Eqs. (4.1), (4.2), (5.9) and (5.10) into Eqs. (5.7) and (5.8), the complete dilation and failure criteria for specimens with varied axial strain rates ($\dot{\varepsilon}$) can be obtained. Figure5.3 compares the criteria with the strength data which shows

good correlations (R^2> 0.8). Parameter m however tends to be independent of the axial

strain rate (Figure 5.4).

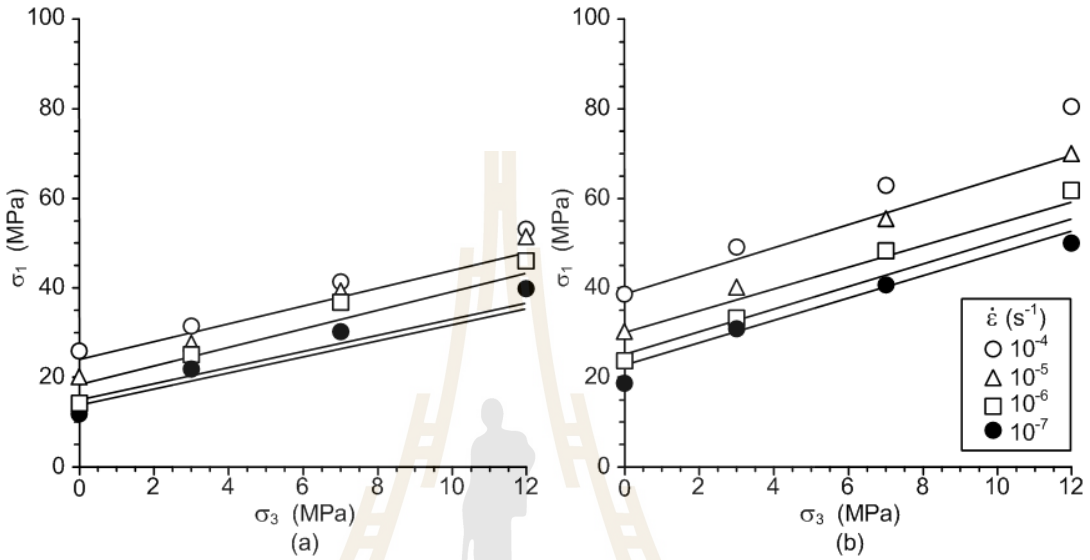

Figure 5.3 Major principal stresses at dilation (a) and at failure (b) as a function of minor principal stress. Hoek-Brown strength criterion fitted to strength data.

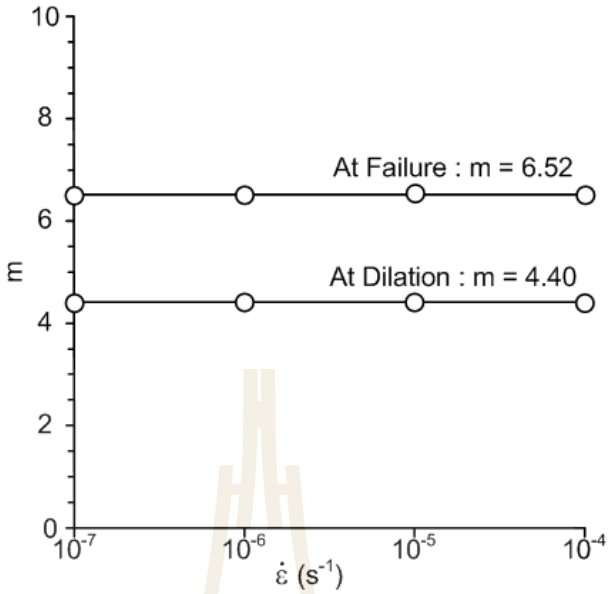

Figure 5.4 Hoek-Brown parameter m as a function of axial strain rates (ε̇).

5.4 Strain energy density criterion

The strain energy density principle is applied to describe the salt strength and deformability under different axial strain rates. A similar approach has been used by Fuenkajorn et al. (2012) to derive a loading rate-dependent strength for salt. The distortionalstrain energy at dilation ($W_{d,d}$) and at failure ($W_{d,f}$) can be calculated from the octahedral shear stresses and strains for each salt specimen using the following relations (Jaeger et al., 2007):

$$W_{d,d} = \frac{3}{2}\int_0^{\gamma_{oct,d}} \tau_{oct,d} \cdot d\gamma_{oct} \tag{5.11}$$

$$W_{d,f} = \frac{3}{2}\int_0^{\gamma_{oct,f}} \tau_{oct,f} \cdot d\gamma_{oct} \tag{5.12}$$

where$\tau_{oct,d}$, $\tau_{oct,f}$ are octahedral shear stresses at dilation and at failure and$\gamma_{oct,d}$, $\gamma_{oct,f}$ are octahedral shear strains at dilation and at failure. The mean stress at dilation ($\sigma_{m,d}$) and at failure ($\sigma_{m,f}$) can be calculated from axial stress (σ_1) and confining pressure (σ_3) for eachsalt specimen using the following relations:

$$\sigma_{m,d} = (\sigma_{1,d} + 2\sigma_3)/3 \tag{5.13}$$

$$\sigma_{m,f} = (\sigma_{1,f} + 2\sigma_3)/3 \tag{5.14}$$

The calculated W_d-σ_m relations at dilation and at failure can be represented by a linear relation, as shown in Figure 5.5. The W_d-σ_m relation above can be used as a

strength criterion, where it implicitly considers the time-dependent strength of the salt.It's therefore more suitable to describe the salt pillar stability, as compared to the conventional strength criteria that exclude thetime-dependent effect.Results for the octahedral shear stresses (τ_{oct}), octahedral shear strains (γ_{oct}), mean stress (σ_m) and distortional strain energy density (W_d) at dilation and at failure are interpreted from these curves and listed in Tables 5.2.

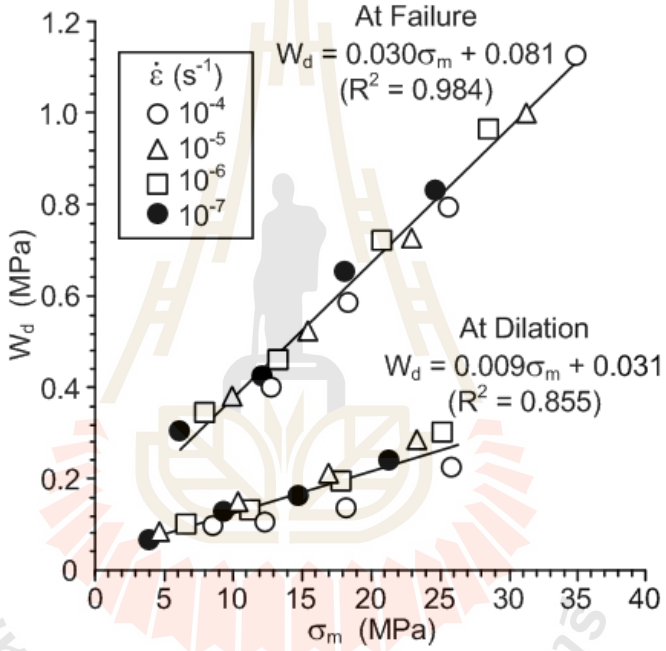

Figure 5.5 Distortional strain energy (W_d) at dilation and at failure as a function mean stress (σ_m).

Table 5.2 Strainenergy of each specimen.

$\dot{\varepsilon}$ (s^{-1})	σ_3 (MPa)	$W_{d,d}$ (MPa)	$\sigma_{m,d}$ (MPa)	$W_{d,f}$ (MPa)	$\sigma_{m,f}$ (MPa)
10^{-4}	0	0.10	8.59	0.40	12.89
	3	0.11	12.45	0.59	18.37
	7	0.14	18.32	0.79	25.64
	12	0.22	25.70	1.13	34.86
10^{-5}	0	0.10	6.69	0.38	10.01
	3	0.13	11.05	0.52	15.37
	7	0.20	17.98	0.72	23.13
	12	0.30	25.14	1.00	31.29
10^{-6}	0	0.08	4.75	0.35	7.89
	3	0.14	10.41	0.46	13.09
	7	0.22	17.08	0.72	20.76
	12	0.28	23.31	0.96	28.55
10^{-7}	0	0.07	4.02	0.30	6.21
	3	0.13	9.28	0.43	12.32
	7	0.16	14.73	0.65	18.30
	12	0.24	21.28	0.83	24.71

CHAPTER VI

PILLAR STABILITIES

6.1 Introduction

The objective of this chapter is to determine the long-term strengths of pillars insalt mines in the MahaSarakham formation, northeast of Thailand based on strain energy density criterion.One of the design requirements is that the pillarsmust remainmechanically stable up to the time of backfill installation.

6.2 Calibration parameters

The objective of the calibration is to determine the properties parameters of thetests. The time-related parameters are monitored, recorded and analyzed. Results from the test provide the data basis for the time-dependent properties of rock salt based on the conventional approach. A simple rheological creep model is used to describe behavior of the salt, i.e., potential creep law.

The total strain in salt can be divided into two parts, elastic strain (linear and recoverable strain) and plastic creep strain (time-dependent and nonrecoverable strain):

$$[\varepsilon^T] = [\varepsilon^e] + [\varepsilon^c] \quad (6.1)$$

where $[\varepsilon^T]$, $[\varepsilon^e]$ and $[\varepsilon^c]$ are three-dimensional vectors of total, elastic and time-dependent plastic strains.

The elastic strain for triaxial compression stress state can be obtained from the generalized Hooke's law the axial (principal) strain can be written as:

$$\varepsilon^e = (\sigma_1 - 2\nu\sigma_3) \tag{6.2}$$

whereε^e is axial strain, σ_1 is axial stress, σ_3 is confining pressure, E is elastic modulus and ν is Poisson's ratio. These elastic parameters can be obtained from relatively quick loading as those performed by Luangthip et al. (2016). They define these parameters as E = 20.23 GPa and ν =0.29.

The plastic creep strain can be derived from the theory of plasticity based on the associated flow rule (Senseny, 1983 and Nair et al., 1974) The equivalent creep strain (ε^{*c}) is first obtained from one dimensional creep law which presents the plastic strain as a function of stress and time (Nair and Boresi, 1970):

$$\varepsilon^{*c} = \varepsilon^e + \kappa\gamma(\frac{2}{3}\sigma^*)^\beta t^{\gamma-1} \tag{6.3}$$

where κ, β and γ are material parameters and $\sigma^*$is equivalent (effective) stress.

Based on the von Mises flow rule, andare defined as:

$$\sigma^* = (1/2)\cdot[(\sigma_1 - \sigma_2)^2 + (\sigma_2 - \sigma_3)^2 + (\sigma_3 - \sigma_1)^2]^{1/2} \tag{6.4}$$

$$\varepsilon^* = (1/2)\cdot[(\varepsilon_1 - \varepsilon_2)^2 + (\varepsilon_2 - \varepsilon_3)^2 + (\varepsilon_3 - \varepsilon_1)^2]^{1/2} \tag{6.5}$$

Substituting equations (6.4) and (6.5) into (6.3) and taking under triaxial stress ($\sigma_2 = \sigma_3$ and $\varepsilon_2 = \varepsilon_3$) we obtain the following:

$$\frac{\sqrt{2}}{3}(\varepsilon_1 - \varepsilon_3) = [(\sigma_1/E) - (2\nu\sigma_3/E)] + \kappa\gamma\left[\left(\frac{\sqrt{2}}{3}\right)\cdot(\sigma_1 - \sigma_3)\right]^{\beta} \cdot t^{\gamma-1} \qquad (6.6)$$

where ε_1 is axial strain, ε_2 is lateral strain, E = 20.23 GPa and ν = 0.29.

Regression analyses on the Equation (6.6) using test data (σ_1, σ_3, ε_1 and ε_3) with the SPSS statistical software (Wendai, 2000) can determine the parameters κ, β and γ for each specimen. Table 6.1 summarizes the potential law parameters for all confining pressures and axial strain rates. The parameters κ, β and γtend to be independent of the axial strain rate and confining pressure as shown in Figure 6.1.

Table 6.1 Potential law parameters based on E = 20.23 GPa and ν = 0.29

Parameters	**σ_3 (MPa)**	**$\dot{\varepsilon}$ (s^{-1})**				**MEAN ± SD**
		10^{-4}	**10^{-5}**	**10^{-6}**	**10^{-7}**	
κ ($\times 10^{-7}$/MPa·s)	0	1.602	1.330	1.209	1.342	1.414 ± 0.19
	3	1.513	1.331	1.599	1.645	
	7	1.257	1.263	1.193	1.519	
	12	1.305	1.272	1.377	1.873	
β	0	2.211	2.310	2.094	2.391	2.219 ± 0.14
	3	2.198	1.986	1.947	2.477	
	7	2.289	2.328	2.221	2.333	
	12	2.234	2.067	2.208	2.206	
γ	0	0.345	0.243	0.243	0.325	0.303 ± 0.06
	3	0.424	0.235	0.324	0.377	
	7	0.357	0.324	0.264	0.233	
	12	0.284	0.244	0.274	0.354	

6.3 Prediction of pillar stabilities

The tributary area concept is applied here to determine the pillar stress (σ_P) for the extraction ratios between 30% and 50%,assuming that the factor of safety (FS.) is 1.0. The pillar stress in terms of the extraction ratio (e) can be written as (Hoek and Brown, 1980):

$$\sigma_P = [(\rho \cdot H)/(1 - e)] \times 100 \qquad (6.7)$$

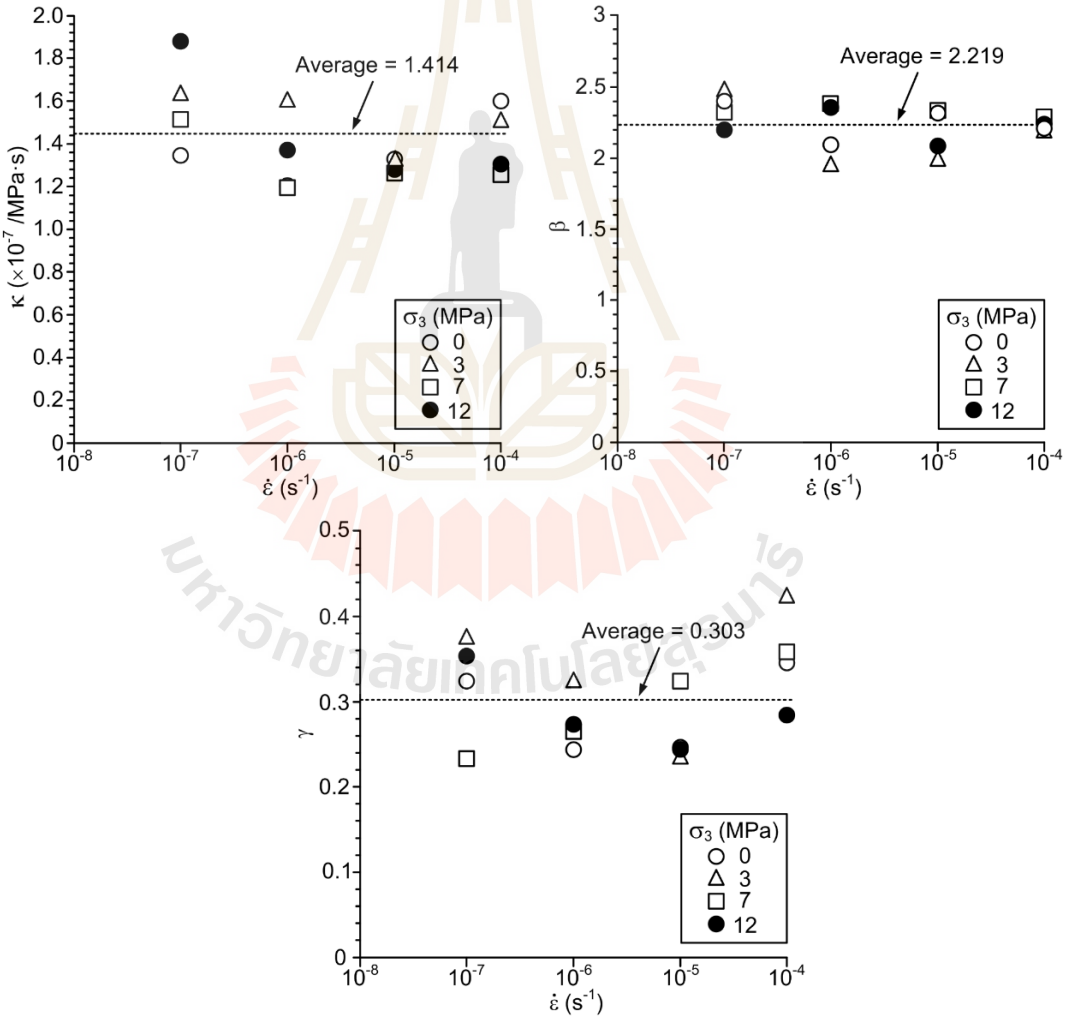

Figure 6.1 Potential law parameters as a function of axial strain rate ($\dot{\varepsilon}$).

where H is the mine depth, and ρ is in-situ stress gradient of overburden (approximated here as 0.027 MPa/m). The calculations are made for the depths from 100 to 400 m.

In order to describe the increase of the pillar deformation (strain) with time under the uniaxial ($\sigma_2=\sigma_3=0$) condition, the potential law in Equation (6.6) can be used. By substituting the material parameters E,κ, β and γ in to Equation (6.3) to determine the pillar strain (ε_P) or axial strain can be rewritten for uniaxial and constant stress condition for each depth and extraction ratio as:

$$\varepsilon_P = (\sigma_P/E) + \kappa \cdot \sigma_P^{\beta} \cdot t^{\gamma} \quad (6.8)$$

A series of axial strain-time curves for salt pillars under various depths and extraction ratios can be developed (Figure 6.2).The pillar strains and their corresponding time at the point where the dilation and failure would occur can be determined by comparing thestresses and time-dependent strains at various pillar ages with the distortional strain energy criterion in Figure 5.5.

The calculated strain energy fordeterminingthe time-dependent strength of pillars for each depth and extraction ratio can be representedfor the distortional strain energy and mean stress at dilation and failure:

$$W_{d,d} = (3/2)\cdot(\tau_{oct}\cdot\gamma_{oct,d}) \quad (6.9)$$

$$W_{d,f} = (3/2)\cdot(\tau_{oct}\cdot\gamma_{oct,f}) \quad (6.10)$$

$$\sigma_{m,d} = \sigma_{P,d}/3 \quad (6.11)$$

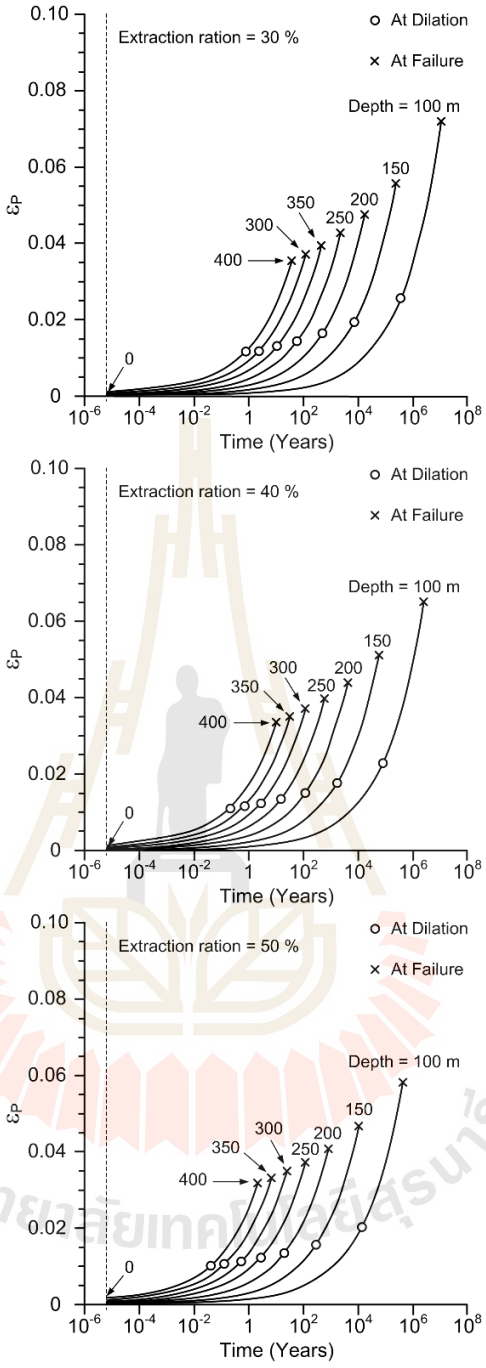

Figure 6.2 Strain time curves under uniaxial condition for each depths and extraction ratios.

$$\sigma_{m,f} = \sigma_{P,f}/3 \quad (6.12)$$

where$\tau_{oct,d}$ is octahedral shear stresses. The pillar stresses at dilation point and at failurepoint are equal. The$\gamma_{oct,d}$ and $\gamma_{oct,f}$values are octahedral shear strains at dilation and atfailurewhich can be calculated by:

$$\tau_{oct,d} = (2/3)\cdot\sigma_P \quad (6.13)$$

$$\gamma_{oct,d} = \frac{\sqrt{2}}{3}\cdot(\varepsilon_{A,d} - \varepsilon_{L,d}) \quad (6.14)$$

$$\gamma_{oct,f} = \frac{\sqrt{2}}{3}\cdot(\varepsilon_{A,f} - \varepsilon_{L,f}) \quad (6.15)$$

where$\varepsilon_{L,d}$ and $\varepsilon_{L,f}$ are lateral strain at dilation and at failure. The axial strain from Equation (6.8) can be used to calculate the lateral strain (ε_L) by relation $\varepsilon_L = -\nu\varepsilon_A$ (usingν =0.29). The relation between the distortional strain energy and mean stress can be obtained from Figure 5.5:

$$W_{d,d} = 0.009\sigma_{m,d} + 0.031 \quad \text{MPa} \quad (6.16)$$

$$W_{d,f} = 0.030\sigma_{m,f} + 0.081 \quad \text{MPa} \quad (6.17)$$

The time at dilation and at failurefrom Equation (6.8) is trialed until the $W_d$reaches the envelopes of dilation and failure.Figure 6.3 shows the time at which the salt pillars reach their dilation and failure points. The results suggest that the duration under stable condition decreases with increasing pillar stresses. The diagrams

can be used as a guideline to ensure that the salt pillars will remain stable up to the time at which the backfill is installed.

6.4 Comparison potential parameter

The objective of the comparison is to determine the parameters from different tests and the times at which the salt pillars reach their dilation and failure point, the strain energy density principle is applied to develop strength criterion for the salt pillars.

Wilalak et al. (2016) perform creep testing on the MahaSarakham formation. Each specimen is tested up to 21 days. The specimens are tested under the axial stresses of 2, 4, 6.5, 13 and 16 MPa. Regression analyses on the strain-time curves based on

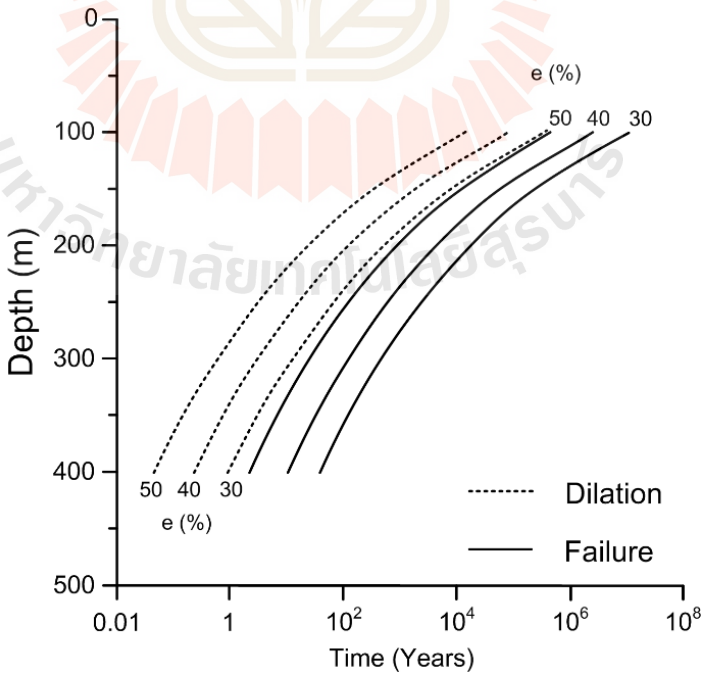

Figure 6.3 Design criteria representing mining depths as a function of time at dilation and at failure.

potential law using the SPSS statistical software (Wendai, 2000) are performed to determine the potential parameters for salt specimen. The Poisson's ratio (ν) is approximated as 0.288. The calibration results are obtained as: elastic modulus (E) = 4.25 GPa, κ = 0.0003 /MPa·day, β = 1.414 and γ = 0.199.

Archeeploha and Fuenkajorn(2013)conducted uniaxial creep tests and cyclic loading test to assess the influence of loading cycles on the time-dependent behavior of the MahaSarakham salt. The constant axial stresses are 6.5, 10, 13, and 16 MPa. After static loading for 21 days the applied stresses are alternated from 0 to the maximum selected stress. Each cycle takes 24 hours. The calibration results are: E = 4.56 GPa, $\kappa = 2.084\times10^{-9}$ /MPa.day, β = 1.434 and γ = 0.188. Define the Poisson's ratio = 0.287 to the calibration parameters.

Khathipphathee (2012) performsthe uniaxial creep test on rock salt.The applied constant axial stresses are 6.5, 9.6, 13.0, 14.8 and 16.0 MPa (about 20% to 50% of the uniaxial compressive strength). The uniaxial creep test is performed under constant temperatures at 0 and 30 degree Celsius. The specimen deformations are monitored along the three principal axes for up to 21 days.The Poisson's ratio (ν) approximate here as 0.29 from Laungthip et al. (2016). The calibration results for ambient temperature (30 degree Celsius) are G = 4.18 GPa, κ = 0.0004 /MPa.day, β = 1.528 and γ = 0.107.Where $G = E/(2(1+\nu))$.

Substituting the material parameters E, ν, κ, β and γ from each test above into Equation (6.3) a series of axial strain-time curves for salt pillars under various depths and extraction ratios can also be developed and compared. The pillar strains and their corresponding time at the point where the dilation and failure would occur can be determined by comparing the stresses and time-dependent strains at various pillar ages with the distortional strain energy criterion in Figure 5.5. Figure 6.4 shows the time at which the salt pillars reach their dilation and failure points for each test. It can be seen that the parameters obtained from the strain rate test here give more conservative results in term of the pillar stability than those obtained from the creep testing.

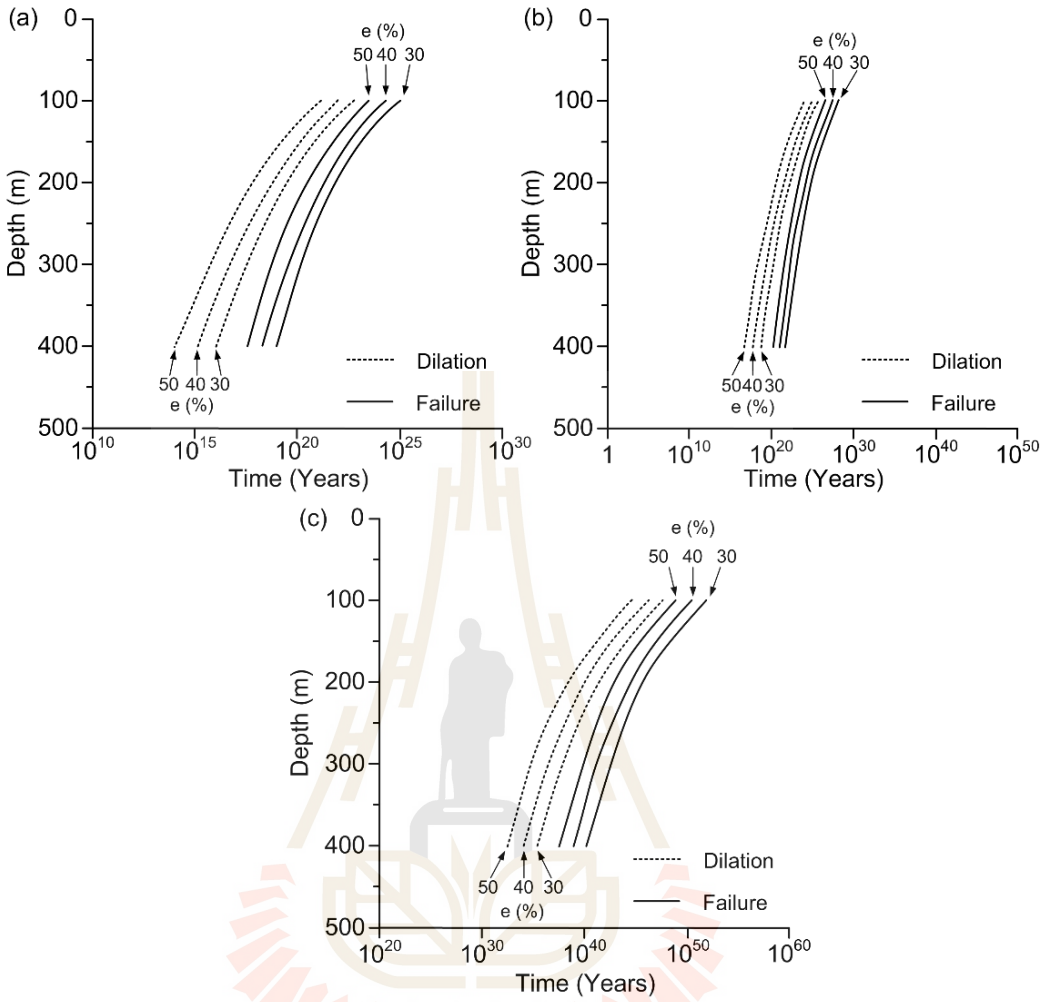

Figure 6.4 Prediction time-dependent strength from uniaxial creep test (Wilalak et al., 2016) (a), uniaxial creep tests and cyclic loading test (Archeeploha andFuenkajorn, 2013) (b)and uniaxial creep test under constant temperatures at 30Celsius(Khathipphathee, 2012) (c)representing mining depths as afunction of time at dilation and at failure.

CHAPTER VII

DISCUSSIONS AND CONCLUSIONS

7.1 Discussions

This section discusses the key issues relevant to the reliability of the test schemes and the adequacies of the test results. Comparisons of the results and findings from this study with those obtained elsewhere under similar test conditions have also been made.

- Goodcoefficients of correlation are obtained for all strain rates and confining pressures, suggesting the reliability of the test procedure.

- The test results agree reasonably well with the test results on the MahaSarakham salt obtained by Sriapai et al. (2012), (2013) and Sartkaew (2013).

- A difficulty is the rate controlling of the applied principal strains to obtain the desired test. A high precision digital pressure and displacement gages are used here while the pressures in the hydraulic pump are manually controlled. Results of the specimens that aresubjected to the strains that deviate for the designed schemes have been discarded.

- The axial strain rate used in this study is relatively high as compared to those of the salt pillar or storage cavern. It is recognized that rock under high strain rate would give higher strength and lower strain than that under lower strain rates(Fuenkajorn and Deamen (1988), Liang et al. (2010), Liang et al. (2007),

Lajtai et al.(1991)andFuenkajorn et al. (2012)). As a results the salt strengths and

theircorresponding criteria derived here may also over-estimate those of the in-situ salt where it is likely to subject to much lower strain rates.

- The distortional strain energy required to dilate and to fail the specimens can be calculated and presented as a function of the mean stress. The specimen under condition of constant confining pressure (σ_3), the distortional strain energy are independent of axial strain rate.

- The advantage of the application of the strain energy criterion over the Coulomb and Hoek and Brown criteria is that it considers both stress and strain at dilation and at failure because rock salt is time-dependent material, and hence their results would be more comprehensive than the Coulomb and Hoek and Brown criteria.

- By calibrating the potential creep law against the test results, the pillar verticalstrain under any vertical stress can be described as a function of time. The pillar distortional strain energy at dilation and at failure can therefore be determined and used to calculate the corresponding strains and time after excavation. The strength criterion based on the strain energy principle is probably more suitable and conservative than the conventional strength criteria. This is because it can incorporate the time - dependent effect by considering both salt strengths and strain at dilation and at failure under various deformation rates. This also suggests that obtaining the salt strengths under a wider range of the strain rates would enhance the representativeness of the proposed strain energy criterion.

7.2 Conclusions

All objectives and requirements of this study have been met. The results of the laboratory testing and analyses can be concluded as follows:

(1) Higher strain rates result in higher peak (failure) strengths, which agree with the experimental results on rock salt performed byFuenkajorn and Deamen (1988), Liang et al. (2010), Dubey and Gairola(2005) and Sriapai et al. (2011). Beyond the dilation point the micro-cracks are probably induced which lead to an increase of the salt specimen volume (Figure 4.4). The specimen laterally dilates beyond the original volume after the peak strength has been reached. A higher strain rate applied results in a higher elastic modulus of the salt.The salt elastic modulus varies from 0.72 to 2.53GPa. The Poisson's ratio from 0.32 to 0.42, and tend to be independent of the applied axial strain rates.

(2) The distortional strain energy required to dilate ($W_{d,d}$) and to fail ($W_{d,f}$) the specimens can be calculated and presented as a function of the mean stress (σ_m). The distortional strain energy decreases with increasing confining pressure. The strain energy criterion agrees well with the strength results from different confining pressure.

(3) This study proposed strength criteria including the Coulomb, Hoek and Brown and the strain energy density criteria. The three criteria can predict the salt strength under various axial strain rate and confining pressure. The strain energy criterion is more conservative as it considers both stresses and strain at dilation and at failure. Nevertheless, derivation of the strain energy criterion requires a more

comprehensive measurements of the stress and strain at dilation or at failure during the laboratory testing.

(4) The simplified approach of pillar design presented here is merely to demonstratethe potential application of the strain energy criterion for the analysis of salt structures. It is based on the tributary area concept while ignoring the shape (height-to-width ratio) size, and end effects. A more comprehensive analysis on these and other relevant factors would be needed to obtain a more realistic design result, which depends upon the site-specific conditions and engineering requirements.

7.3 Recommendations for future studies

Recognizing that the numbers of the specimens and the test parameters used here are limited, more testing and measurements are recommended, as follows:

(1) Larger specimen size should be used to enhance the representativeness of the test results. This is invoked by the scale effect that that normally occurs when laboratory test results are applied to the in-situ conditions.

(2) Different strain rates should be used in the test to assess the rate-dependent strength of the salt. The strain rate effects should explicitly include in the strength criteria.

(3) Verification of the accuracy of the proposed criteria should be made by comparing with the actual salt opening stability.

(4) The effect of temperature should be assessed in the laboratory. The specimens should be tested under the range of temperatures expected to occur in the salt around the openings.

(5) Increasing the number of the specimens would statistically enhance the reliability of the test results and the predictability of the proposed strength criterion.

REFERENCES

Allemandou, X. and Dusseault, M. B. (1996). Procedures for cyclic creep testing of salt rock, results and discussions. In **Proceedings of the Third Conference on the Mechanical Behavior of Salt** (pp. 207-218). Clausthal-Zellerfeld: Trans Tech Publications.

Archeeploha, S. and Fuenkajorn, K. (2013). Effects of cyclic loading on creep behavior of MahaSarakham salt. In **Proceedings of the Fourth Thailand Symposium on Rock Mechanics** (pp. 91-98). NakhonRatchasima, Thailand.

Artkhonghan, K. and Fuenkajorn, K. (2015). Effects of Stress Path on Polyaxial Strengths of MahaSarakham Salt. **Vietrock 2015 an ISRM specialized conference.** 12-13 March 2015, Hanoi, Vietnam.

ASTM D7012-07. Compressive strength and elastic moduli of intact rock core specimens under varying states of stress and temperatures. **Annual Book of ASTM Standards** (Vol. 04.08). Philadelphia: American Society for Testing and Materials.

ASTM D7012-07. Compressive strength and elastic moduli of intact rock core specimens under varying states of stress and temperatures. **Annual Book of ASTM Standards** (Vol. 04.08). Philadelphia: American Society for Testing and Materials.

ASTM D7070-08. Standard test methods for creep of rock core under constant stress and temperature. **Annual Book of ASTM Standards** (Vol. 04.09). American Society for Testing and Materials.

Aubertin, M., Julien M. R., Servant, S. and Gill, D. E. (1999). A rate-dependent model for the ductile behavior of salt rocks. **Canadian Geotechnical Journal** 36(4): 660-674.

Aubertin, M., Sgaoula, J. and Gill, D. E. (1992). A damage model for rock salt: Application to tertiary creep. In **the Seventh Symposium on Salt** (vol. 1, pp. 117-125). Elsevier Science Pub.

Aubertin, M., Sgaoula, J. and Gill, D. E. (1993). Constitutive modeling of rock salt: Basic considerations for semi-brittle behavior. In **Proceedings of the Fourth International Symposuim on Plasticity and It's Current Applications** (pp. 92). Baltimore.

Aubertin, M., Sgaoulla, J., Servant, S., Julien, M. R., Gill, D. E. and Ladanyi, B. (1998). An upto-date version of SUVIC-D for modeling the behavior of salt. In **Proceedings of the Fourth Conference on the Mechanical Behavior of Salt** (pp. 205-220). Clausthal, Germany: Trans Tech Publications.

Bieniawski, Z. T. and Bernede, M. J. (1978).Suggested methods for determining theuniaxial compressive strength and deformability of rock materials. InternationalJournal of Rock Mechanics and Mining Sciences 16(2): 138-140.

Chokski, A. H. and Langdon, T. G. (1991). Characteristics of creep deformation in ceramics. **Materails Science and Technology** 7: 577-584.

Dubey, R. K., and Gairola, V. K. (2005). Influence of stress rate on rheology-An experimental study on rock salt of Simla Himalaya, India. **Geotechnical and Geological Engineering** 23: 757-772.

Dusseault, M.B. and Fordham, C.J. (1993). Time-dependent behavior of rocks. **Comprehensive Rock Engineering Principles, Practice and Project: Rock Testing and Site Characterization** (Vol. 3: pp. 119-149). London.

Farmer, I. W. (1983). **Engineering behavior of rock. 2nd Edition**.Chapman and Hall, New York.

Fokker, P. A. (1995). The behavior of salt and salt caverns. **Ph.D Thesis,** Delft University of Technology.

Fokker, P. A. (1998). The micro-mechanics of creep in rock salt. In **Proceedings of the Fourth Conference on the Mechanical Behavior of Salt** (pp. 49-61). Clausthal-Zellerfeld, Germany: Trans Tech Publications.

Fokker, P. A. and Kenter, C. J. (1994). The micro mechanical description of rock salt plasticity. **In Eurock'94** (pp. 705-713). Rotterdam: Balkema.

Fuenkajorn, K, Sriapai, T., and Samsri, P. (2012). Effects of loading rate on strength and deformability of MahaSarakham salt. **Engineering Geology** 135-136: 10-23.

Fuenkajorn, K. and Daemen, J. J. K. (1988). Boreholes closure in salt. **Technical Report Prepared for The U.S. Nuclear Regulatory Commission. Report No. NUREG/CR-5243 RW.** University of Arizona.

Hoek E., Carranza-Torres C. and Corkum B. (2002). Hoek-Brown failure criterion-2002 edition. **Proceedings of the fifth North American rock mechanics symposium** (pp 267–273). Canada, Toronto.

Hoek, E. and Brown, E.T. (1980). Empirical strength criterion for rock masses. **Journal of Geotechnical and Geoenvironmental Engineering** 160(GT9): 1013-1035.

Hyder, Z., Ali, Z., Akram, M., Westman, E. and Karmis, M. (2011). Simulation and modeling of pillar stability and analysis of safety factor. **SME Annual Meeting & Exhibit and CMA 113th National Western Mining Conference 2011.** 27 February-2 March, Denver, Colorado, USA.

Jaeger, J. C., Cook, N. G. W. and Zimmerman, R. W. (2007). **Fundamentals of Rock Mechanics, 4th edition**. Blackwell publishing, Oxford.

Jaeger, J. C., Cook, N. G. W. and Zimmerman, R. W. (2007). **Fundamentals of Rock Mechanics, 4th edition**. Blackwell publishing, Oxford.

Jaeger, J.C., and Cook, N.G.W. (1979). **Fundamentals of Rock Mechanics, 3rd edition**.Chapman & Hall, London.

Jeremic, K. L. (1994). **Rock Mechanics in Salt Mining** (530 pp.). Rotherdam: A. A. Balkema.

Khathipphathee, T. (2012). Effects of low temperatures on strength and time-dependent deformation of rock salt. Master Degree Thesis, Suranaree University of Technology, NakhonRatchasima, Thailand.

Knowles, M. K., Borns, D., Fredrich, J., Holcomb, D., Price, R. and Zeuch, D. (1998). Testing the disturbed zone aroud a rigid inclusion in salt. In **Proceedings of the Fourth Conference on the Mechanical Behavior of Salt** (pp. 175-188). Clausthal, Germany: Trans Tech Publications.

Lajtai, E. Z., Duncan, E. J. S., and Carter, B. J. (1991). The effect of strain rate on rock strength. **Rock Mechanics and Rock Engineering** 24: 99-109.

Langer, M. (1984). The Rheological behavior of rock salt, Mechanical behavior of salt I. In **Proceedings of the First Conference on the Mechanical Behavior of Salt** (pp. 201-240). Clausthal-Zellerfeld, Germany: Trans Tech Publications.

Lau, L. I. H.(2010). Performance of Pillars in Rock Salt Mines. **Master degree thesis**, University of Waterloo in fulfillment of the thesis requirement for the degree of Master of Applied Science in Civil Engineering. Waterloo, Ontario, Canada.

Liang, W. G., Zhao, Y. S., Xu, S. G. and Dusseault, M. B. (2011). Effect of strain rate on the mechanical properties of salt rock. **International Journal of Rock Mechanics & Mining Sciences** 48: 161-167.

Liang, W., Yang, C., Zhao, Y., Dusseault, M.B. and Lui, J. (2007). Experimental investigation of mechanical properties of bedded salt rock. **International Journal of Rock Mechanics and Mining Sciences** 44: 400-411.

Luangthip, A., Khamrat, S. and Fuenkajorn, K. (2016). Effects of carnallite contents on stability and extraction ratio of potash Mine. **9th Asian Rock Mechanics Symposium.** 18 - 20 October 2016, Bali, Indonesia.

Munson, D. E. and Wawersik, W. R. (1993). Constitutive modeling of salt behavior – State of the technology. In **Proceedings of the Seventh International Congess on Rock Mechanics** (vol. 3, pp. 1797-1810). Balkema.

Nair, K. &Boresi, A. (1970). Stress analysis for time-dependent problems in rock mechanics. **Proceedings of the 2nd Congress of the International Society for Rock Mechanics** (pp. 531-536), Belgrade.

Nair, R.S., Chang, C-Y, Singh, R. D. and Abdullah, A. M. (1974). Time-dependent analysis to predict closure in salt cavities. **Proceedings of the 4th Symposium on Salt** (pp. 129-139). Cleveland, Ohio.

Sambeek, V. and Leo, L. (1997). Salt pillar design equation. **16th International Conference on Ground Control in Mining** (Chapter 29). Morgantown, August 5-7.

Sartkaew, S. and Fuenkajorn, K. (2013). Effect of stress rate on uniaxial compressive strength of rock salt under 0-100^{o} C. **The 11th International Conference on Minerals and Petroleum Engineering** (pp 53-61).

Senseny, P. E. (1983). **Review Of Constitutive Laws Used To Describe The Creep Of Salt** (45 pp.). Battelle Memorial Institute, Columbus, Ohio.

Sriapai, T. (2010). **True Triaxial Compressive Strengths OfMahaSarakham Rock Salt.** Master Degree Thesis, Suranaree University of Technology, NakhonRatchasima, Thailand.

Sriapai, T., Samsri, P. and Fuenkajorn, K. (2011). Influence of loading rate on compressive strength of rock salt. In **Proceedings of the Third Thailand Symposium on Rock Mechanicson** (pp. 117-124). NakhonRatchasima, Thailand.

Sriapai, T., Walsri, C. and Fuenkajorn, K. (2012). Effect of temperature on compressive and tensile strengths of salt. **ScienceAsia**38: 166-174.

Thongprapha, T., Khamrat, S. and Fuenkajorn, K. (2016). Determination of safe withdrawal rates of compressed-air energy storage caverns in MahaSarakham salt. **9th Asian Rock Mechanics Symposium.** 18 - 20 October 2016, Bali, Indonesia.

Wendai, L. (2000). Regression analysis, linear regression and probit regression In 13 chapters. **SPSS for Windows: statistical analysis.** Publishing House of Electronics Industry. Beijing.

Wilalak, N. and Fuenkajorn, K. (2016). Constitutive equation for creep closure of shaft and borehole in potash layers with varying carnallite contents. **9th Asian Rock Mechanics Symposium.** 18 - 20 October 2016, Bali, Indonesia.

BIOGRAPHY

Miss. Prapasiri Junthong was born on July 25, 1991 in Bangkok, Thailand. She received his Bachelor's Degree in Engineering (Geological Engineering) from Suranaree University of Technology in 2015.For her post-graduate, she continued to studywith a Master's degree in the Geological Engineering Program, Institute of Engineering,Suranaree university of Technology.During graduation, 2015-2017, she was a part timeworker in position of research assistant at the Geomechanics Research Unit, Institute ofEngineering, Suranaree University of Technology.